

# Nobel Lecture: Sub-atomic motions\*

Ferenc Krausz<sup>†</sup>

*Ludwig-Maximilians-Universität München, Munich, Germany,  
Max-Planck-Institut für Quantenoptik, Garching, Germany,  
and Center for Molecular Fingerprinting Research, Budapest, Hungary*

 (published 28 August 2024)

The written version of my lecture is a personal reflection on decades of research on electron-light interactions, culminating in their control and observation in real time at the turn of the millennium. Electrons and light attracted my attention when attending the lectures of György Marx on quantum mechanics and Károly Simonyi on electrodynamics during the 1980s in Budapest. This interest was solidified by my mentor, Arnold Schmidt, and deepened by Paul Corkum, during the 1990s in Vienna. They have influenced my path most profoundly. It has been a tremendous privilege to stand on the shoulders of scientists, including many Nobel laureates, who made seminal contributions to our understanding of electrons and light, when walking the path to exploring sub-atomic motions. To eventually exploit them for addressing grand challenges. To the benefit of humankind.

DOI: [10.1103/RevModPhys.96.030502](https://doi.org/10.1103/RevModPhys.96.030502)

## CONTENTS

I. We Are Electrons!	1	XXVII. Other Paths	20
II. Sub-atomic Scales—and Motions	1	Acknowledgments	21
III. Light Particles, Matter Waves	2	References	21
IV. What Is Motion in Atomic Dimensions? On Which Timescale Does It Typically Occur?	2		
V. How to Observe Sub-atomic Motions in Real Time	3	<b>I. WE ARE ELECTRONS!</b>	
VI. Temporal Confinement via Nonlinearities	4	The world that we can observe is made of atoms. Atoms, in turn, are made of a nucleus and electrons bound to it. Outside nuclear reactors (and meanwhile nuclear batteries), nuclei are effectively passive. Beyond defining the mass of bodies, they are merely spectators of all the actions undertaken by electrons. In our biological and modern life, likewise. So far immeasurably small, yet furnished with a finite mass and electric charge, <sup>1</sup> these elementary particles define the functionality of matter. Inorganic and organic matter likewise.	
VII. From Electrical Pulses to Pulses of Light	4	Electrons are ubiquitous. It is hard to imagine that it wasn't until 125 years ago that humankind became aware of their existence. And it took more than another 100 years to capture their motion in their natural home: within atoms, molecules, solids.	
VIII. Controlling the Electric Field of Light	5		
IX. Toward an Isolated Attosecond Event	5	<b>II. SUB-ATOMIC SCALES—AND MOTIONS</b>	
X. The Birth of an Isolated Attosecond Pulse	6	The atomic length scale is deduced from the van der Waals volume of atoms ( <a href="#">van der Waals, 1910</a> ) as hundreds of picometers. Dynamics within these dimensions are referred to as <i>sub-atomic motions</i> .	
XI. Precision Attosecond Control and Metrology	8	These motions initiate biochemical processes that create and maintain life. They govern the exchange of energy between light and matter, underlying future signal processing at optical rates. Creating and harnessing sub-atomic motions with light collects information about the health state of living	
XII. Initiating and Tracing Sub-atomic Motions	10		
XIII. A Hole Deep Inside an Atom—What Happens after Its Creation?	11		
XIV. Behind Chemical Bonds and Electric Signals—Valence Electrons	12		
XV. Sub-atomic Tunneling Resolved in Time	12		
XVI. Sub-atomic Electron Oscillations in Slow Motion	12		
XVII. From Isolated Atoms to Condensed Matter	14		
XVIII. Sub-atomic Motions in Condensed Matter: Electric Polarization	14		
XIX. Light-Matter Energy Transfer in Real Time	14		
XX. Petahertz Real-Time Oscilloscope	15		
XXI. Attosecond Condensed-Matter Science	17		
XXII. Probing Molecules via Sub-atomic Electronic Motions	17		
XXIII. EMF versus NMR	17		
XXIV. Sub-atomic Motions Probe Human Health	17		
XXV. Toward Caring for Health—By Monitoring it	19		
XXVI. Our Path	19		

\*The 2023 Nobel Prize for Physics was shared by Pierre Agostini, Ferenc Krausz, and Anne L'Huillier. This paper is the text of the address given in conjunction with the award.

<sup>†</sup>I would like to dedicate this article to Professor Arnold Schmidt, Technische Universität Wien, who passed away on July 5, 2024. His guidance and mentorship greatly influenced my path described in this article.

<sup>1</sup>The electron's rest mass is less than half a thousandth of that of a proton, the nucleus of the hydrogen atom. Its electric charge is equal to that of the proton, but opposite (negative) in sign.

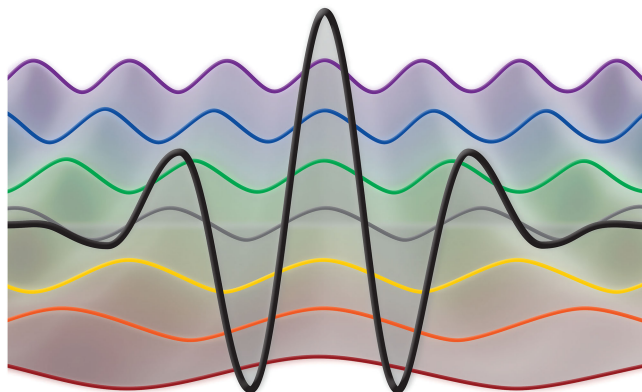


FIG. 1. Waves of different wavelength can create a wave packet highly localized in space (as well as in time) when being added to each other with proper phase.

organisms. And may allow much more than we can possibly envision now.

### III. LIGHT PARTICLES, MATTER WAVES

A century ago, Arthur Compton’s discovery of inelastic scattering of x-rays off electrons (Compton, 1923) revealed that light quanta carry both a momentum given by

$$\mathbf{p} = \hbar \mathbf{k} \quad (1)$$

and an energy given by

$$E = \hbar \omega. \quad (2)$$

These findings provided compelling arguments for the existence of light particles, dubbed “photons.” In Eqs. (1) and (2),  $\mathbf{p}$  and  $\mathbf{k}$  denote the momentum (as a vector, with direction and magnitude) of the light particle, photon, and the wave vector of the light beam, respectively, and “omega” the angular frequency of its field oscillations.

Inspired by the dual appearance of light, obeying as waves Maxwell’s wave equations, and accounting for the Compton effect as particles carrying momentum and energy, de Broglie established the same connection (de Broglie, 1929) as given by Eq. (1) between the motion of the particle and the propagation of the associated wave with  $p = mv/\sqrt{[1 - (v/c)^2]}$  describing the relativistic momentum of the particle, where  $v$  is its velocity, and with  $k = 2\pi/\lambda$  giving the angular wave number of the wave associated with the particle [see also Compton (1923)]. Shortly thereafter, the wave nature of the electron along with Eq. (1) was experimentally verified via electron diffraction (Davisson and Germer, 1927; Thomson and Reid, 1927).

The wave nature of electrons naturally resolves the mystery about why electrons do not spiral into the tiny nucleus, but rather form a stable atom with a size some 10 000 times larger than the size of its nucleus. If the electron is a wave, its localization (around the atomic nucleus) requires the superposition of electron waves with many different wavelengths (i.e. wave numbers), as shown in Fig. 1. This is a consequence of the mathematical fact that any function—in this case the hypothetical electron wave function surrounding the atomic

nucleus depicted by the black line in Fig. 1—can be constructed by adding perfectly periodic functions of different periods.

Increasing confinement calls for adding waves with decreasing wavelength, i.e., increasing wave numbers. This, in turn, implies—according to Eq. (1)—increasing the spread of electron momenta. This counteracts stronger confinement, preventing thereby the implosion of the electron cloud around the nucleus.

The electron as a wave prompted Erwin Schrödinger to create his celebrated wave equation (Schrödinger, 1926, 1933). Quantum mechanics was born. Arguably one of the most impactful achievements of modern science.

### IV. WHAT IS MOTION IN ATOMIC DIMENSIONS? ON WHICH TIMESCALE DOES IT TYPICALLY OCCUR?

In the macroscopic world, motion is described by its trajectory, the variation of the position of an object over time. The uncertainty principle prevents us from describing motion with trajectories on the atomic scale. What to do? Max Born proposed and proved (Born, 1954) that the modulus square of the wave function gives the probability,  $|\psi(x, y, z)|^2 dx dy dz$ , with which a suitable measurement would find the electron in the infinitesimal volume  $dx dy dz$ . Any change of this probability in time,  $|\psi(x, y, z, t)|^2$ , results in the *rearrangement of the probability distribution of the electron*, which is the closest analogy to motion in the macroscopic world.

The textbook example for sub-atomic motion is represented by the superposition of the  $1s$  and  $2p$  states of the hydrogen atom, which can be created by exposing an ensemble of hydrogen atoms to a stream of the ultraviolet photons with the energy  $E_{\text{ph}} = \hbar \omega = E_{2p} - E_{1s}$  (10.2 eV, 121.6 nm). Some of them will be resonantly absorbed and excite atoms from the  $1s$  ground state to the  $2p$  excited state. After the photon stream passed the interaction volume, a fraction equal to  $|c_{1s}|^2$  of all the atoms will be in the  $1s$  state and a fraction equal to  $|c_{2p}|^2$  will be in the  $2p$  state ( $|c_{1s}|^2 + |c_{2p}|^2 = 1$ ), in line with the statistical interpretation of the wave function. If we performed a measurement on any individual atom, we would find it with a probability of  $|c_{1s}|^2$  and  $|c_{2p}|^2$  in the  $1s$  and  $2p$  states, respectively.

Figure 2 shows snapshots of the electron probability distribution,  $|\psi(x, y, z, t)|^2$  for  $|c_{1s}|^2 = |c_{2p}|^2 = 0.5$ , at different instants of the  $1s$ - $2p$  superposition state of the electron in the hydrogen atom.

The  $1s$ - $2p$  superposition state creates a dipole oscillating at the frequency of

$$\nu_{1s-2p} = \frac{1}{T_{1s-2p}} = \frac{E_{2p} - E_{1s}}{2\pi\hbar} \quad (3)$$

corresponding to an oscillation period of

$$T_{1s-2p} = 405 \text{ as} = 16.755 \text{ atomic units of time}$$

with  $1 \text{ as} = 10^{-18} \text{ s}$ .

*Quantum mechanics uncovers the characteristic timescale for sub-atomic motions, the motion of electrons in atomic dimensions. It is the attosecond timescale.*

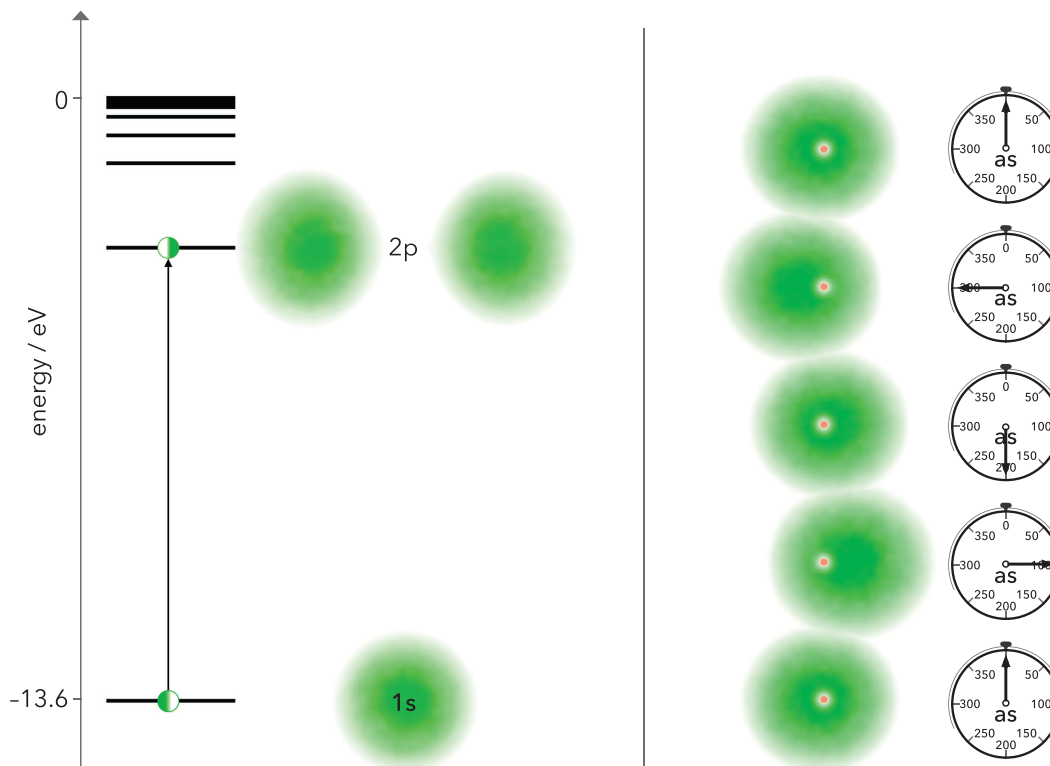


FIG. 2. Energy levels of the hydrogen atom and modulus square of the wave function of the  $1s$  and  $2p$  states represented by clouds (left-hand side). Temporal evolution of the  $1s$ - $2p$  superposition state with time elapsing from the bottom to the top of the figure (right-hand side).

Almost a century had passed since the first hint at the existence of an elementary unit of charge from Faraday's electrolysis (Faraday, 1834), until the nature of its carriers and the physical laws governing their behavior were understood. It took almost another century to develop the ability to observe their dynamics in sub-atomic dimensions.

## V. HOW TO OBSERVE SUB-ATOMIC MOTIONS IN REAL TIME

Capturing ultrafast processes requires control of some interaction with the process under scrutiny within the natural timescale of its evolution. For electrons slow compared to the speed of light (and that's what we shall be concerned with), the electric field mediates the required interaction. The fastest field variations that we can control with a bandwidth comparable to the carrier frequency are oscillations of visible and infrared laser light.

If these field oscillations could drive some highly nonlinear process, exhibiting an extreme sensitivity to the field strength, the nonlinear process could be confined to tiny intervals near the peaks of the oscillating electric field. Unfortunately, these peaks occur every half cycle and hence a large number of times in a typical laser pulse.

Let us consider a laser pulse with an electric field as depicted in Fig. 1. Here, the field strength at the pulse peak is *significantly* stronger than anywhere else in the pulse. A nonlinear process driven by this field comes into being merely in the closest proximity of this *isolated* peak. Starting shortly

before it. And ending shortly thereafter. For visible-near-infrared light, existing within a time interval of hundreds of attoseconds. Short enough to resolve the “prototypical” sub-atomic motion shown in Fig. 2. These considerations prompted the following grand questions:

Is the generation of strong electric-field waveforms of visible-infrared light featuring a single half cycle that peaks significantly higher than any other one feasible? (**Q1**)

Could single-cycle light produce an *isolated* attosecond event, and could these tools enable the observation of electron phenomena in real time? (**Q2**)

Is attosecond-resolution/precision probing feasible within *condensed matter*? If yes, which applications appear to be most rewarding? (**Q3**)

They crystallized out, one after the other, between 1990 and 2010, defined the agenda for our work and helped set priorities properly: **Q1** for the 1990s, **Q2** for the 2000s, and **Q3** from 2010 on, until the present day. The quest for answers serves as an organizing principle for the rest of this manuscript.

Before we turn our attention to addressing **Q1**, the quest for “light waveforms with a single strongest oscillation peak,” we briefly review how brief electric signals came into being and allowed the birth of high-speed electronics. It will be instructive to see that the concepts underlying the generation

and measurement of brief electrical pulses in modern electronics also underlie

**attosecond physics: the control and measurement of light waves and attosecond pulses, and their use for observing and controlling electron motion in atomic dimensions (Krausz and Ivanov, 2009).**

## VI. TEMPORAL CONFINEMENT VIA NONLINEARITIES

The most efficient way of producing fields oscillating at a multitude of frequencies is to drive electric current under conditions when it grows ever steeper for increasing voltage. Physicists refer to this behavior as “nonlinear.” A textbook example for a nonlinear electronic component is the *semiconductor diode*. It is widely used in modern electronics, both as a stand-alone device and as a key functional element of transistors (Bardeen, 1956). Acting like a one-way valve for electric current, a diode allows current to flow only for positive voltages, with a magnitude increasing exponentially with the applied voltage (as shown in Fig. 3). For negative voltages, the current is negligible.

Contemporary semiconductor electronics enable—via nonlinearities—the control of electronic current on a picosecond timescale with microwave fields in nanoscale circuits. The resultant ultrafast electrical pulses constitute the basis for real-time observation of periodic and transient electronic signals up to 100 GHz and beyond, in modern sampling and real-time oscilloscopes. In what follows, we shall see how, analogously, nonlinear electric currents driven by optical fields underlie light wave electronics, the technological basis for experimental attosecond physics.

Optical-field-induced nonlinear electric currents originate from the universal response of transparent matter (atoms, molecules, solids) to strong electric fields of (sufficiently) low-frequency light: tunneling ionization. The seminal work of Keldysh revealed a universal exponential dependence of the current emerging due to the release of electrons from atoms or from the valence band of wide-gap solids (Keldysh, 1964) via tunneling driven by a slowly-varying optical field.

The generation of picosecond electrical and attosecond electron pulses, from which picosecond THz and attosecond deep-UV/extreme ultraviolet (XUV) light pulses can be derived, are based on the same principles. Apply a fast-oscillating electric field to a nonlinear device. Microwaves oscillate at frequencies up to about 100 GHz. Optical fields oscillate at frequencies of hundreds of THz. Driving the current by a microwave field can result in picosecond pulses. Driving the current by a light field can result in attosecond pulses. The basic underlying concept is the same in both cases. The “device” is an electric circuit in the former case and an atom or an insulating solid in the latter case, leading to electric currents in circuits and atoms on picosecond-nanometer and attosecond-picometer scales, respectively.

But how to transfer the technical capability of precisely controlling microwave electric fields to visible-infrared light

fields, at frequencies many thousand times higher than the frequency of contemporary electronics, in order to create light wave electronics?

This was the challenge to which I devoted the first one and a half decades of my professional life. Together with a small team of highly talented and most dedicated researchers, at the Technical University of Vienna. And with the generous support and wise guidance of my mentor, Professor Arnold Schmidt.

## VII. FROM ELECTRICAL PULSES TO PULSES OF LIGHT

Extending coherent radiation toward optical frequencies became possible with the discovery of atomic and molecular light amplifiers (Townes, 1964) by Charles Townes, Nicolay Basov, and Aleksandr Prokhorov in the 1950s. In 1960, Theodor Maiman realized the first visible laser (Maiman, 1960).

Figure 1 demonstrates the basic concept for the synthesis of an ultrashort light pulse. Let the continuous waves represent different longitudinal modes of a laser resonator. If the phases of these modes are locked to each other, an ultrashort pulse (typically much longer than the one depicted in Fig. 1 though) emerges—as a result of a short-lived constructive interference between the modes—and circulates in the laser resonator, at a repetition rate,  $f_r$ .

But how to enforce laser mode locking? Just as *nonlinear currents* induced by microwave electric fields underlie the generation of electrical pulses, the *nonlinear polarization* induced by the electric field of laser light (Bloembergen, 1981) has been crucial for the formation of ultrashort pulses within a laser and their further shortening after amplification.

For moderately strong electric fields, the electric polarization can be written as

$$P_i(t) = \chi_{ij}^{(1)} E_j(t) + \chi_{ijk}^{(2)} E_j(t) E_k(t) + \chi_{ijkl}^{(3)} E_j(t) E_k(t) E_l(t) + \dots \quad (4)$$

where  $\chi^{(n)}$  stands for the linear (first-order), the second- and third-order nonlinear susceptibilities for  $n = 1, 2, 3$ , respectively, and  $i, j, k, l$  represent one of the Cartesian components  $x, y$ , or  $z$  of the polarization of the electric field, respectively. For simplicity, the susceptibilities are assumed as independent of the optical frequency.

The third-order nonlinear susceptibility implies a correction to the refractive index of transparent materials, referred to as the optical Kerr effect. It is proportional to the instantaneous intensity of the laser pulse,

$$\Delta n \propto \chi^{(3)} I(r, t), \quad (5)$$

introducing a radial ( $r$ ) and temporal ( $t$ ) dependence of the refractive index. They cause self-focusing and self-phase modulation of the laser light, respectively. Both play a central role in the generation of ultrashort laser pulses.

When introduced in a laser resonator, the former effect may—for increased intensity—reduce the loss that the laser

radiation suffers upon its circulation in the cavity. This fosters the growth of an initial intensity fluctuation and the simultaneous decay of the continuous-wave “background” in the resonator. In the steady state, the continuous-wave radiation completely disappears. What remains is an ultrashort pulse circulating in the resonator. Kerr-lens mode-locked operation is achieved (Spence, Kean, and Sibbett, 1991), first demonstrated in a titanium-doped sapphire (Ti:sapphire) laser (Moulton, 1986).

Precise control of the intracavity group-delay dispersion across the entire gain bandwidth could be first accomplished by chirped multilayer mirrors (Fig. 4), pioneered by Robert Szipőcs and Kárpát Ferencz from Budapest and first applied in a laser by Andreas Stingl and Christian Spielmann, the first experimentalists under my supervision (Stingl *et al.*, 1994; Szipőcs *et al.*, 1994). These chirped multilayer mirrors are now ubiquitous, integral parts of any femtosecond laser and experiments using ultrashort pulses.

External amplification of these ultrabrief pulses requires temporal stretching before boosting the pulse energy and subsequent temporal compression to avoid excessive intensities in the laser amplifier (Strickland and Mourou, 1985). The energy of ultrashort laser pulses could thereby be boosted to the millijoule level and beyond, but also elongated them to 20–30 fs duration. To shorten these energetic pulses, they were first self-phase modulated in a gas-filled hollow-core fiber and subsequently temporally compressed by chirped mirrors (Fig. 5). A joint Milan-Budapest-Vienna effort spawned the first powerful near-single cycle, henceforth briefly: *single-cycle* light pulses (Nisoli *et al.*, 1997). Powerful enough to ionize atoms.

For such short pulse durations, comparable to the field oscillation cycle, a parameter that did not make any difference in the interaction of matter with multicycle radiation: the carrier-envelope phase, denoted by  $\varphi$  in Fig. 5, becomes important. Changing its value from zero to  $\pi/2$  turns a waveform with a single strongest oscillation peak (half cycle) in the center of the pulse into one with two somewhat weaker, equally strong peaks pointing up and down before and after the center of the pulse. Laser physicists call them a “cosine” and “sine” waveform, respectively. Such a change remains without consequence in the interaction of a multicycle light pulse with matter. By contrast, for the single-cycle pulses depicted in Fig. 5, a shift in  $\varphi$  causes a significant change in the evolution of highly nonlinear electron processes (such as tunneling) driven by these fields. A lack of control of  $\varphi$ , as was the case in femtosecond technology, needed to be fixed.

### VIII. CONTROLLING THE ELECTRIC FIELD OF LIGHT

Laser mode locking yielded femtosecond pulses with reproducible parameters. Except for the carrier-envelope phase  $\varphi$ , the behavior of which was unknown until the mid-1990s. The waveform control of laser pulses was first accessed in 1996 by Lin Xu and Christian Spielmann (Xu *et al.*, 1996).  $\varphi$  was found to shift by an uncontrolled amount,  $\Delta\varphi$ , from one pulse to the next in the train of pulses delivered by a mode-locked laser. I reported about this observation in a colloquium at the Max-Planck-Institute of Quantum Optics. After the talk, Theodor Hänsch informed me about his group’s

efforts to control the frequency comb of a femtosecond Ti:sapphire laser.

It became clear that there is a connection. For a comb of equidistant eigenfrequencies of the longitudinal modes  $f_n = f_0 + nf_r$  a simple analysis yields

$$\Delta\varphi = 2\pi \frac{f_0}{f_r}. \quad (6)$$

Let’s suppose that the spectrum of the laser can be broadened to a full octave (Russell, 2003). The second harmonic of the low-frequency spectral components of the laser pulse generated via the second-order nonlinear susceptibility,  $\chi^{(2)}$ , in a nonlinear medium yields coherent radiation that overlaps in frequency with the high-frequency wing of the pulse. Its radio-frequency spectrum consists of the same frequency comb except for its offset frequency, which is  $f_n^{(2\omega)} = 2f_0 + nf_r$ . Hence, the superposition of the frequency-doubled low-frequency light with the highest-frequency portion of the fundamental spectrum will exhibit a slow modulation of its overall amplitude (physicists call it “beating”) at  $f_n^{(2\omega)} - f_n = f_0$ . Measuring this beating signal and locking it to a radio-frequency reference permits full control of  $\Delta\varphi$  according to Eq. (6) (Hänsch, 2005).

Combining this technique with powerful single-cycle pulse generation (Fig. 5), Andrius Baltuska and Thomas Udem realized the first strong laser fields with controlled evolution (Baltuska *et al.*, 2003). A broadband laser along with  $\chi^{(2)}$  and  $\chi^{(3)}$  nonlinearities allowed **Q1** to be answered in the affirmative. We could now set out to address **Q2**: does the concentration of electromagnetic energy in a single oscillation period of visible-near-infrared light permit the generation of an isolated attosecond event?

### IX. TOWARD AN ISOLATED ATTOSECOND EVENT

As discussed above, a highly nonlinear process—such as tunneling ionization, depending on the field strength similarly as plotted in Fig. 3—driven by a single-cycle optical field may give rise to it. However, an attosecond-duration electron emission from an ensemble of atoms is of limited utility for time-resolved science. Paul Corkum’s three-step model

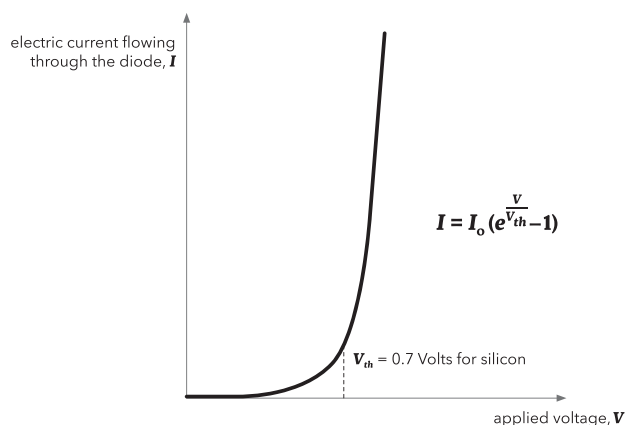
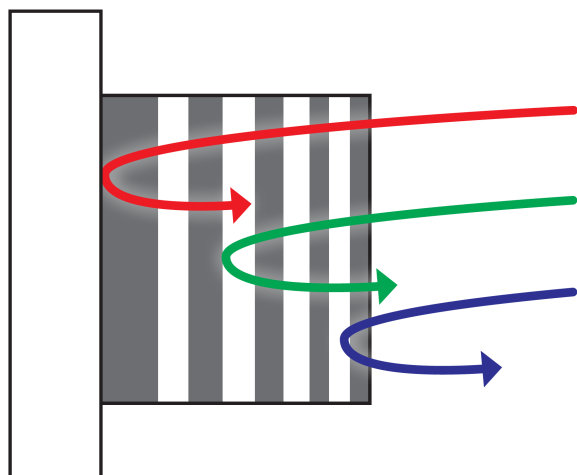


FIG. 3. Electric current ( $I$ ) flowing through a semiconductor diode when a voltage  $V$  is applied to it.



chirped multilayer mirror

FIG. 4. Group-delay control in a chirped multilayer mirror. Narrowband wave packets carried at different wavelengths penetrate to different depths before being reflected, as a consequence of a modulation of the multilayer period across the layer stack. In the illustrating example, the increasing multilayer period with increasing distance from the mirror surface implies that radiation with increasing wavelength has to penetrate deeper before being reflected. The result is a group delay that raises with increasing wavelength, which is needed in laser oscillators and pulse compressors to compensate for the frequency sweep (chirp) imposed on the ultrashort laser pulses by material dispersion and self-phase modulation.

(Corkum, 1993) suggested that an inherent concomitant of tunneling ionization induced by a linearly-polarized infrared laser field is the emission of XUV light. In the form of

high-order harmonics of multicycle laser light, discovered by Anne L’Huillier and co-workers (Li *et al.*, 1989). We applied the Corkum-Lewenstein model (Lewenstein *et al.*, 1994) to describe high-harmonic emission from neon atoms ionized by single-cycle laser pulses. Figure 6 summarizes the underlying physical picture and the essential predictions.

The computations of Vladislav Yakovlev and Armin Scrinzi [Fig. 6(e)] suggest the emission of an *isolated* attosecond pulse or *twin* pulses of XUV light at the highest photon energies emitted (cutoff radiation) for a “cosine”-shaped ( $\varphi = 0$ ) and “sine”-shaped ( $\varphi = \pi/2$ ) version of the pulses available in the experiments described by Baltuska *et al.* (2003), respectively. In agreement with the experimentally-observed spectra, shown in Fig. 6(d). The emergence of an isolated attosecond XUV pulse from ionizing atoms with single-cycle laser light was predicted several years before the experimental demonstration by Ivan Christov and co-workers (Christov, Murnane, and Kapteyn, 1997).

## X. THE BIRTH OF AN ISOLATED ATTOSECOND PULSE

Ever since the discovery of high-order harmonics of laser light in the late 1980s, laser pulses consisting of many (or at least several) field oscillation cycles have been used for their generation. Christian Spielmann and co-workers were the first to generate high-order harmonics with single-cycle laser pulses light (Spielmann *et al.*, 1997). It took another few years to measure the temporal structure of the emission.

To this end, we constructed—in cooperation with Markus Drescher, Ulf Kleineberg, and Ulrich Heinzmann from Bielefeld—a vacuum beamline, sketched in Fig. 7.

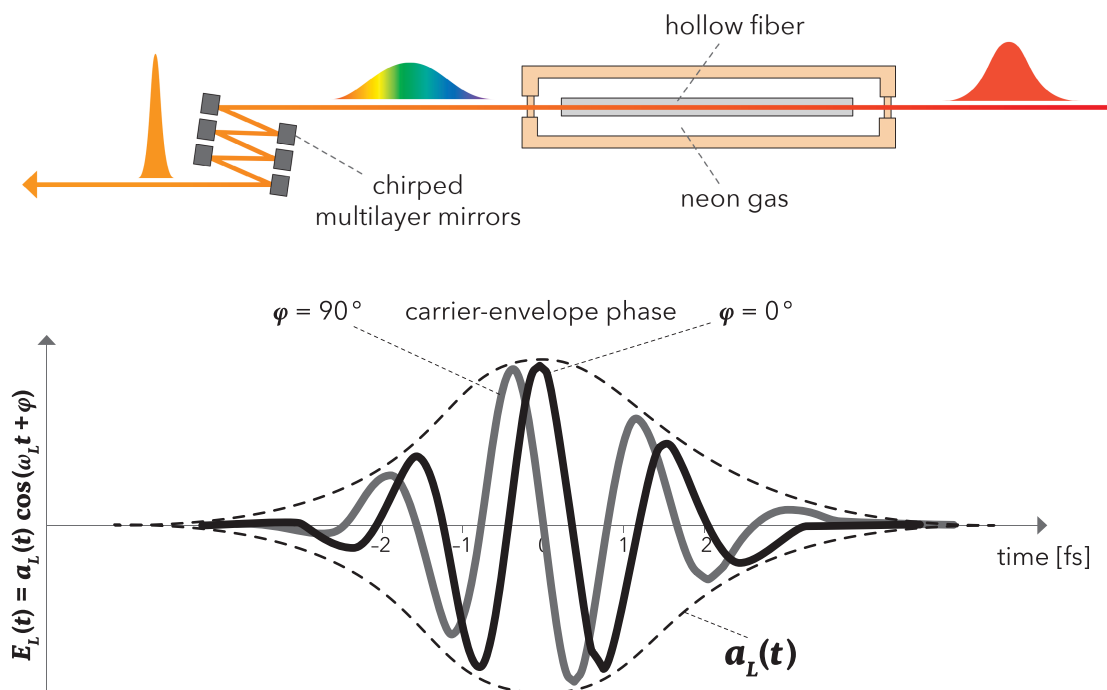


FIG. 5. Self-phase modulation due to the optical Kerr effect in a gas-filled hollow-core fiber broadens the spectrum of a high-energy ultrashort laser pulse. At the output, the pulse carries a frequency sweep and can be temporally compressed by chirped multilayer mirrors. Bottom panel: near-single-cycle light pulses generated by the two steps.

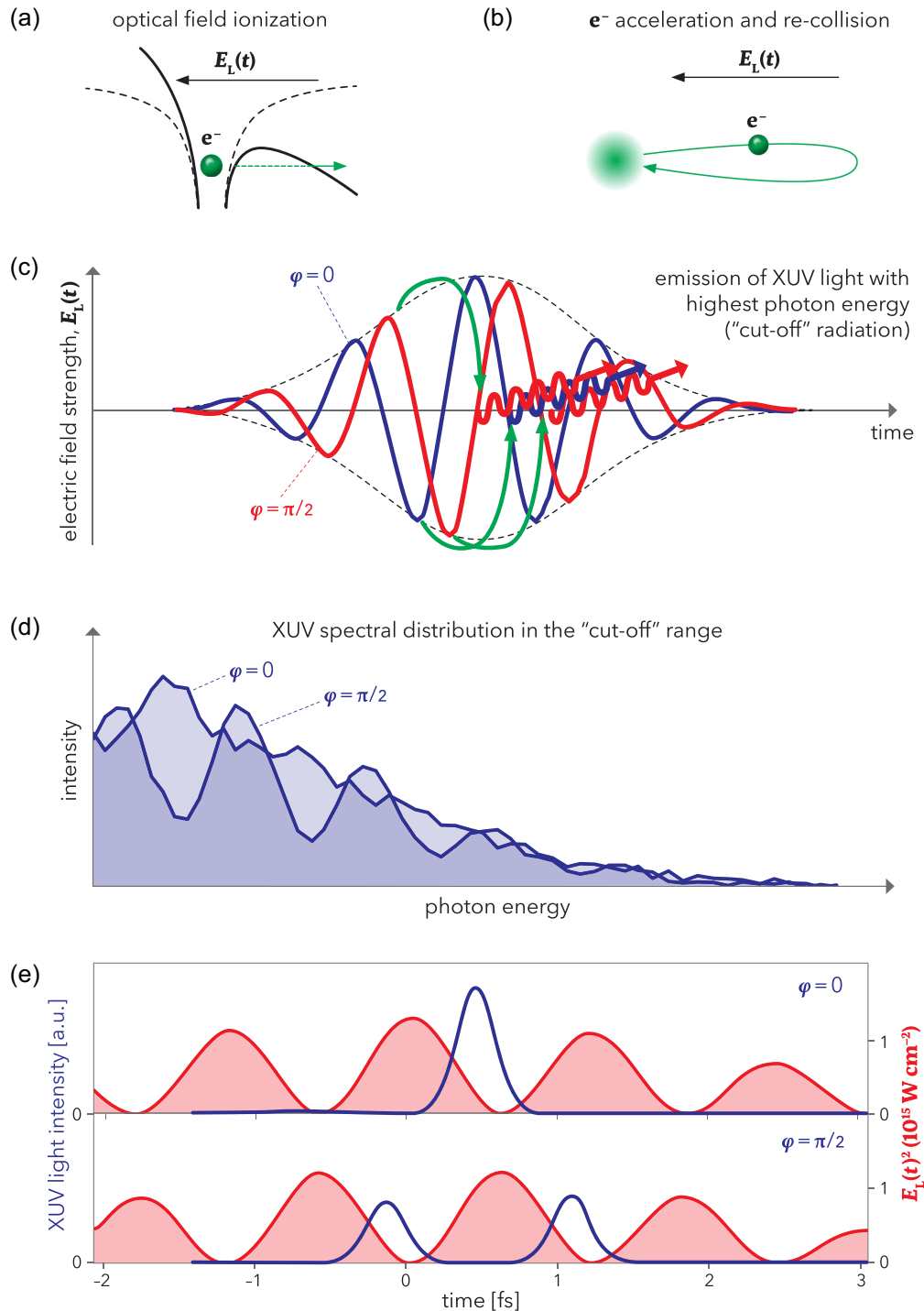


FIG. 6. Physical picture of high-order harmonic generation in a rare gas exposed to a single strong electric-field cycle of near-infrared laser light (Baltuska *et al.*, 2003), based on the three-step model of Corkum (1993). Step 1. (a): The Coulomb potential binding valence electrons to the atomic core (dashed curve) is temporarily suppressed at moments around the field oscillation peak. An electron tunnels through the suppressed potential barrier (solid curve), leaving a hole in the most-weakly-bound atomic orbital. The breaking free electron forms a wave packet temporally confined to a small fraction of this half period (lasting about 1.2 fs at a wavelength of 750 nm) owing to the highly nonlinear—Fig. 3—like—dependence of the ionization probability on the field strength. Step 2. (b): The freed electron is initially pulled away from the nucleus and then pushed back to it by the linearly polarized laser electric field. Step 3. (b): Upon return to the nucleus, the traveling wave packet overlaps with the static bound-state portion of the wave function of the same electron. This overlap results in rapid dipole oscillations, leading—with substantial probability—to the emission of an XUV photon. (c) The trajectories of electrons recolliding with the highest energy (green lines), occurring twice for a sine-shaped ( $\varphi = \pi/2$ ) and once for a cosine-shaped ( $\varphi = 0$ ) driving waveform. (d) The experimental spectra at the highest photon energies generated with single-cycle laser pulses for a cosine and a sine waveform in the experiments described by Baltuska *et al.* (2003). The smooth and modulated spectrum is in accordance with the theoretical prediction of an isolated attosecond XUV pulse and twin pulses, respectively, at the highest photon energies, which is shown in (e).

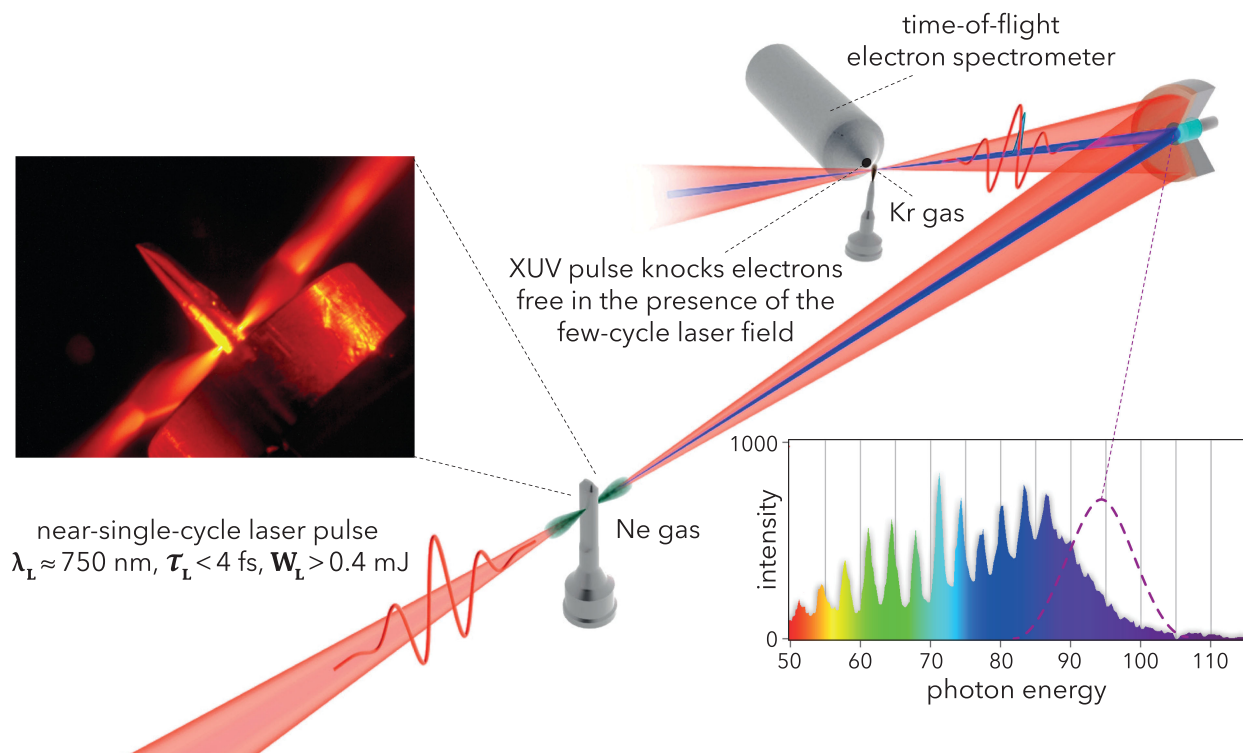


FIG. 7. Schematic illustration of the experimental apparatus that permitted the generation and measurement of the first isolated sub-femtosecond pulses in 2001 at the Technical University of Vienna. Photo courtesy of Gabriel Tempea.

Single-cycle laser pulses ionized neon atoms to produce high harmonics, which copropagate with the driving laser beam. The two coaxial beams are then focused onto a second gas target of krypton atoms by a concentric piezo-controlled double mirror unit. The central Mo/Si reflector focuses the 90-eV XUV harmonics, and a bandpass filter selects the highest-energy photons as indicated in the harmonic spectrum.

In the second gas target, the XUV pulses knock off photoelectrons from krypton atoms in the presence of the laser field. A time-of-flight spectrometer analyzed the momentum distribution of the electrons ejected perpendicularly to the direction of the laser field. Depending on the moment of their release, the photoelectrons are deflected to a varying extent by the laser field. In September 2001, Michael Hentschel and Reinhard Kienberger observed a pronounced modulation of the momentum distribution versus delay and evaluated a 650 as average duration of the XUV pulses hitting the Kr atoms. “Average” because the carrier-envelope phase of the laser pulses was not yet stabilized, making only the average temporal extension of the XUV pulses accessible in this study.

## XI. PRECISION ATTOSECOND CONTROL AND METROLOGY

Single-cycle laser pulses with a controlled electric-field evolution opened the door for the reproducible generation of isolated attosecond XUV pulses and their use for the time-resolved study of electron phenomena. The very first task was the characterization of the new tools.

To this end, the two collinear beams delivering the laser and XUV pulses were again focused in a gas target of krypton atoms (Fig. 7). The XUV pulses again hit the atoms in the

presence of the laser field, but this time the time-of-flight tube was aligned parallel to the direction of the laser electric field (Fig. 8). This allowed the collection and momentum measurement of the electrons that were catapulted from the atoms along the laser polarization.

Depending on their moment of release with respect to the laser oscillations—the electrons are accelerated or decelerated by the field. The temporal profile of the XUV pulse is thereby mapped to a final momentum distribution of photoelectrons [Fig. 9(a)]. Recording this XUV-induced and laser-streaked

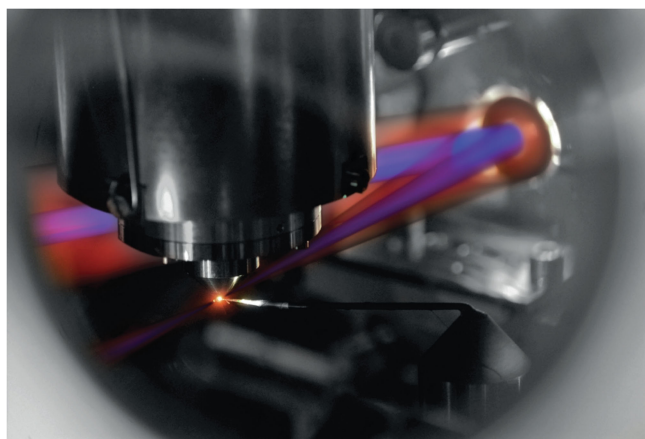


FIG. 8. The common focus of the single-cycle laser beam and the attosecond XUV pulse defines the interaction region, where electron processes are initiated and probed by analyzing the emitted photoelectrons or secondary electrons with a time-of-flight spectrometer. Courtesy of Thorsten Naeser and Christian Hackenberger.

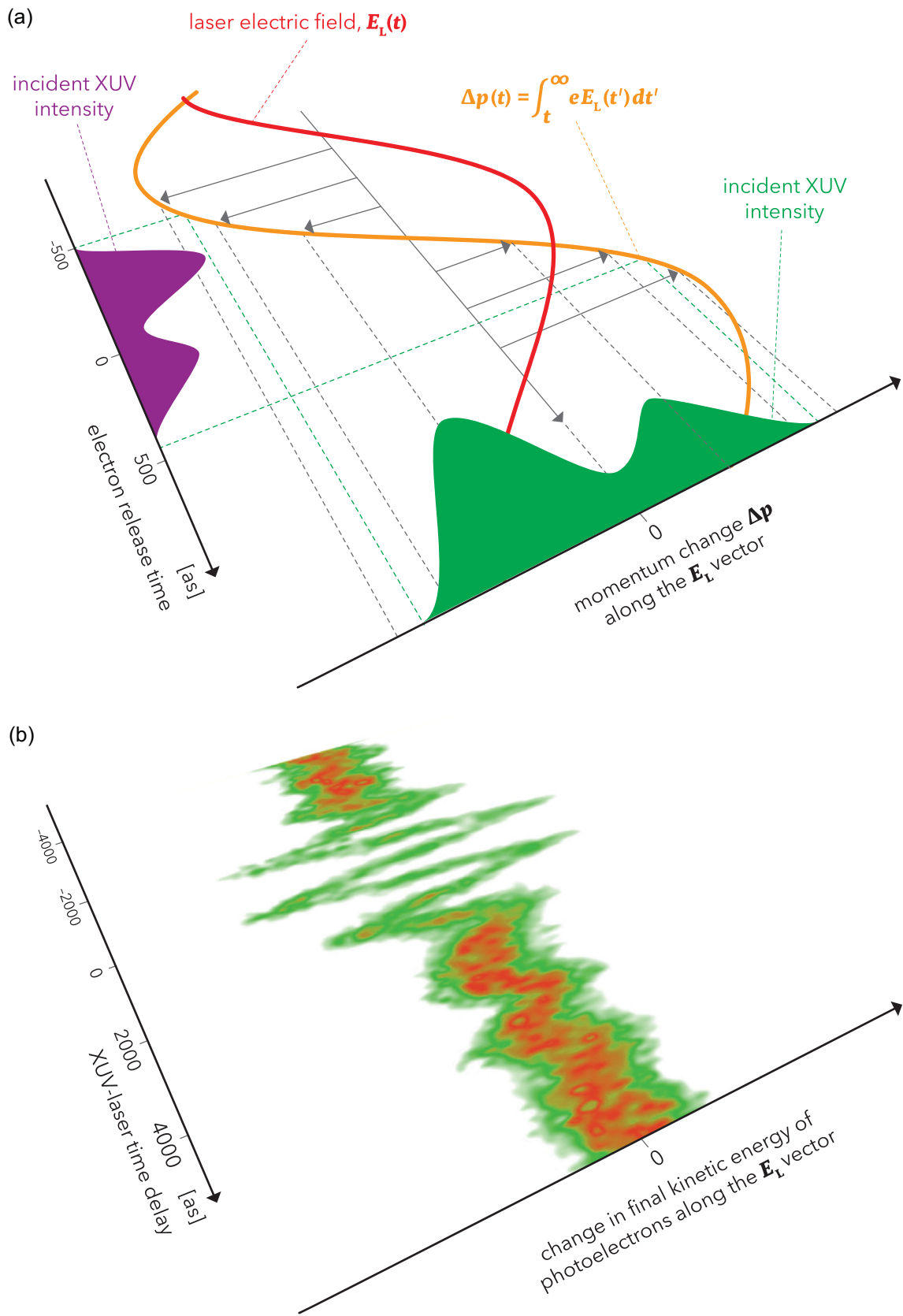


FIG. 9. Concept and implementation of light-field-driven attosecond streaking. (a) Change of the photoelectrons' momentum (arrows) released by an attosecond XUV pulse at a fixed delay in the presence of a strong laser field (red line). (b) Variation of the final photoelectron momentum distribution as a function of delay of the XUV pulse with respect to the streak laser field.

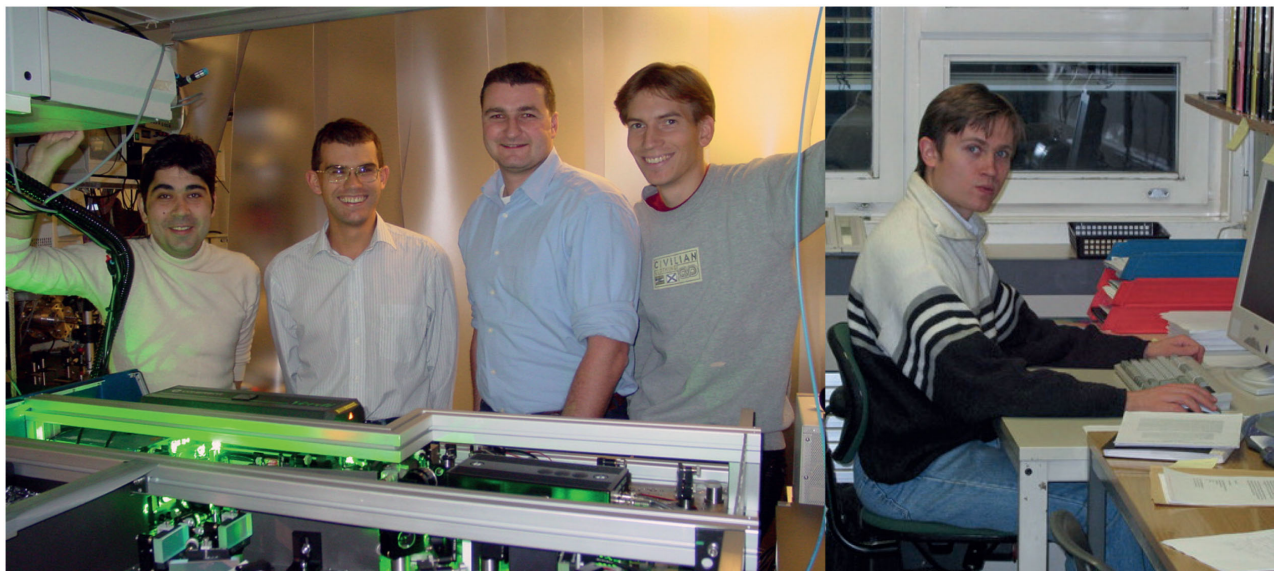


FIG. 10. The heroes behind the first precision attosecond measurements by use of the controlled electric-field oscillations of visible-near-infrared laser light. From left to right: Eleftherios Goulielmakis, Andrius Baltuska, Reinhard Kienberger, Matthias Üiberacker, and Vlad Yakovlev at the Technical University of Vienna in 2004.

photoelectron spectrum as a function of delay results in a spectrogram [Fig. 9(b)]. It allows complete retrieval of *both* the laser waveform *and* the complex amplitude of the attosecond XUV pulse.

The underlying concept is analogous to that of a cathode-ray streak camera. The concept of the light-field-driven attosecond streak camera was proposed by Paul Corkum and theoretically described simultaneously by Jiro Itatani and co-workers (Itatani *et al.*, 2002) and Markus Kitzler and co-workers (Kitzler *et al.*, 2002). Attosecond streaking was first implemented by Reinhard Kienberger, Eleftherios Goulielmakis, Matthias Uiberacker, Andrius Baltuska, and Vladislav Yakovlev in Vienna (Goulielmakis *et al.*, 2004; Kienberger *et al.*, 2004; see Fig. 10). They demonstrated, this time on an attosecond timescale, how *control enables observation*. This control meanwhile extends to timescales well below 100 as (Fig. 11) (Goulielmakis *et al.*, 2008) and the reconstruction of the single-cycle field and the attosecond XUV pulse from the streaking spectrogram shown in Fig. 9(b)

is well understood (Mairesse and Quéré, 2005; Yakovlev *et al.*, 2010).

## XII. INITIATING AND TRACING SUB-ATOMIC MOTIONS

With the controlled attosecond-varying electric force and synchronized attosecond-duration isolated pulse in place, one could set out to using them for real-time observation and control of electron-light phenomena.

Depending on the binding energy of the electron under scrutiny, the motion can be started with the XUV pulse or with the strong laser field. Electrons with a binding energy of several tens of electronvolts (or more) can only be excited/freed by XUV/x-ray photons. Loosely bound (valence) electrons with a binding energy of the order of 10 eV (or less), in turn, can be “energized” by a strong visible/infrared laser field via tunneling or multiphoton-induced transitions. High-energy (inner-shell) electronic excitations are relevant for x-ray lasers. Low-energy (outer-shell) electrons, in turn,

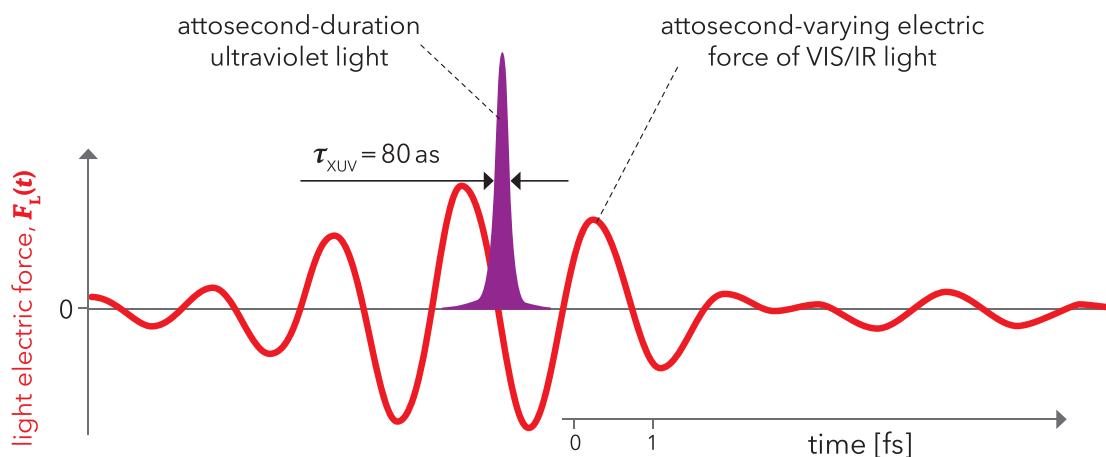


FIG. 11. Tools of attosecond control and metrology with sub-100-as resolution (Goulielmakis *et al.*, 2008).

play a key role in molecules and in modern semiconductor electronics.

### XIII. A HOLE DEEP INSIDE AN ATOM—WHAT HAPPENS AFTER ITS CREATION?

Electrons have been released from the inner shells of atoms since the early days of x-ray spectroscopy, pioneered by Moseley (Moseley, 1913) and Siegbahn (Siegbahn, 1925). Subsequent advances yielded precise values of x-ray spectral linewidths, indicative of few-femtosecond-to-sub-femtosecond lifetimes of inner-shell holes in atoms (Krause and Oliver, 1979). Their direct measurement was not possible until the turn of the new millennium.

Sub-atomic motion was first studied in isolated atoms (Drescher *et al.*, 2002). An attosecond XUV pulse abruptly liberated an electron from an inner shell of krypton atoms; see Fig. 12(b). The created vacancy was rapidly filled with an electron from an outer shell, which transferred its excess energy to another outer electron that was thereby ejected from the atom; see Fig. 12(c). The process was independently discovered by Lise Meitner and Pierre Victor Auger in 1922 and 1923, respectively. Eighty years later, the birth of attosecond science allowed measuring the lifetime of an inner-shell vacancy, by its creation with an attosecond XUV pulse and via simultaneous attosecond streaking of concomitant

valence electron emission and the resultant Auger-Meitner electron emission (Drescher *et al.*, 2002).

Inner-shell ionization implies a variety of multielectron processes mediated by electron-electron interactions (Fig. 12) (Uiberacker *et al.*, 2007).

Attosecond streaking and attosecond tunneling spectroscopy interrogates the *population dynamics of (quasi)stationary quantum states* triggered by the absorption of an energetic photon from an incident attosecond pulse. This also causes a rearrangement of the electron cloud around the nucleus, but in a way very different from the cloud dynamics in Fig. 2, which occurs at constant level populations.

Attosecond streaking has also enabled the simultaneous probing of electrons ejected from different quantum states of the same atoms (Schultze *et al.*, 2010) or from different states of a solid target (Cavalieri *et al.*, 2007). The resultant measurements of relative photoemission delays provide real-time insight into *10-as-scale electron-electron interactions* in atoms and *angstrom-scale electron transport* in solids, respectively. The latter is yet another example of *sub-atomic motion*, this time within one or two atomic layers underneath the surface of a solid sample (Cavalieri *et al.*, 2007) or through atomic layers deposited on the surface (Neppel *et al.*, 2015).

Sub-atomic motions can not only be triggered by the ejection of an inner-shell electron but can also be directly initiated in the external shells of atoms, as we shall see in the next section.

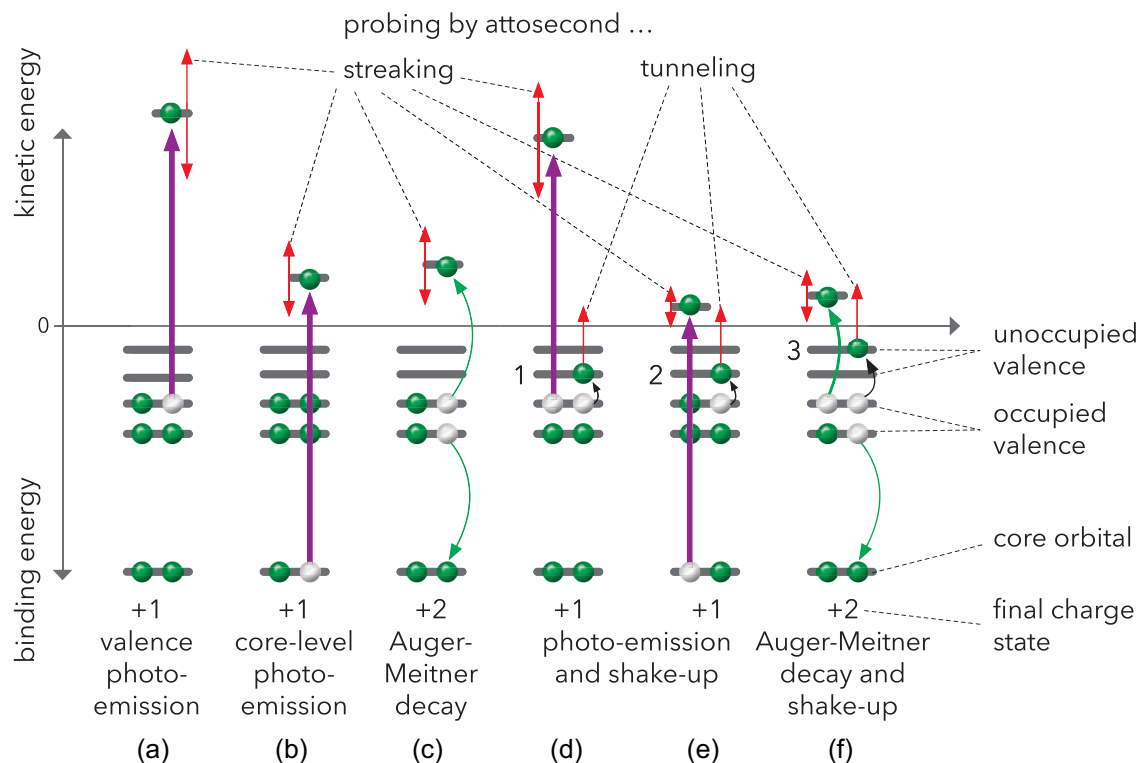


FIG. 12. Probing electron dynamics in atoms, molecules, or solids with attosecond spectroscopy. An attosecond XUV/x-ray pulse initiates the motion by catapulting an electron from (a) an outer or (b) a core shell. The temporal evolution of the emission of a photoelectron or (c) an Auger-Meitner (A-M) electron is probed by attosecond streaking. The photoelectron emission uncovers the evolution of the XUV intensity and the laser electric field, whereas the A-M electron provides information about inner-shell relaxation. The liberated electron may promote [black arrows in (d), (e), and (f)] another electron to unoccupied levels (1, 2, 3). A strong field can probe the population of shake-up levels by tunneling ionization.

#### XIV. BEHIND CHEMICAL BONDS AND ELECTRIC SIGNALS—VALENCE ELECTRONS

The most loosely bound electrons in atoms, molecules, and in band-gap solids are called *valence* electrons. They are of the utmost importance for our life. For our biological and everyday life, likewise. The former relies on molecules, the latter on modern electronics. Molecules are formed and disintegrated by the motion of valence electrons—via the formation and breakup of chemical bonds. And electronic signals are being processed via the motion of valence electrons induced by microwave electric fields in nanoscale integrated circuits via the motion of valence- and conduction-band electrons induced by microwave electric fields in integrated semiconductor circuits.

To set valence electrons going, one needs to transfer them sufficient energy to overcome the several-eV energy barrier to higher energy levels, in atoms, molecules, or band-gap solids (semiconductors or insulators). If we wish to observe the unfolding motion in real time, the excitation must happen within a fraction of a femtosecond. This can be implemented either by resonant excitation with an attosecond ultraviolet pulse or via tunneling with a single-cycle infrared laser pulse.

Isolated attosecond ultraviolet pulses were born (Heinzerling *et al.*, 2024) almost simultaneously with the announcement of the 2023 Nobel Prize in Physics. In combination with single-cycle infrared light—they are opening unprecedented avenues to controlling and probing electron dynamics on molecular orbitals and in the valence and conduction bands of solids.

In the history of attosecond science, triggering valence electron motion was first realized via strong-field-induced tunneling. The following sections are devoted to this route for real-time observation of valence electron dynamics in atoms and band-gap solids.

#### XV. SUB-ATOMIC TUNNELING RESOLVED IN TIME

One of the first triumphs of quantum mechanics was the theoretical description of field emission, i.e., the emission of electrons from a metal into vacuum, induced by a static electric field orthogonal to the metal surface. Fowler and Nordheim have shown that electrons captured within a rectangular potential well can escape with finite probability once the barrier becomes suppressed by a static external field,  $E$ , resulting in a *rate of electron liberation* that depends exponentially on the applied field strength (Fowler and Nordheim, 1928),  $w \propto e^{-a/E}$ . Here  $a$  is a factor depending on the work  $W_b$  the electron would have to do to break free classically, above the barrier. The field-induced promotion of electrons from the valence to the conduction band of semiconductors/insulators or of atomic electrons into vacuum are other forms of field emission. In all cases, the electrons must traverse a classically forbidden region of space, which has been referred to as quantum tunneling, briefly: *tunneling*.

In a seminal work, Keldysh (1964) described the phenomenon in oscillating electric fields, which was later refined by Ammosov, Delone, and Krainov (ADK) (Ammosov, Delone, and Krainov 1986). Keldysh introduced an adiabaticity parameter,  $\gamma$ , which is proportional to the laser frequency

and inversely proportional to the peak electric field of the laser,  $E_{\text{peak}}$ . If  $\gamma$  is much smaller than 1, the temporally-varying tunnel ionization rate then nearly adiabatically follows variations of the oscillating optical field,

$$w(t) \propto e^{-a/|E(t)|}. \quad (7)$$

For  $E_{\text{peak}}$  sufficiently strong to allow valence electrons to break free, this adiabatic regime is predicted to be approached at frequencies in the near-infrared spectral range. Equation (7) then predicts tunneling ionization to be substantially confined to a temporal interval of several hundred attoseconds near the oscillation peak(s) of the laser field.

Experimental verification of this prediction from the 1960s had to wait until 2011, when optical-field-induced tunnel ionization of krypton atoms could be probed with isolated attosecond XUV pulses by Adrian Wirth, Mohammed Hassan, Eleftherios Goulielmakis, and co-workers in Garching (Fig. 13) (Wirth *et al.*, 2011).

Figure 13 reveals how optical-field-induced tunneling in krypton atoms is evolving within the central half cycle of a cosine-shaped near-infrared laser waveform, which was measured simultaneously by attosecond streaking (see Figs. 7 and 9). It takes the electron about 700 as to break free, via tunneling through the barrier formed by the Coulomb attraction of the nucleus and the strong external field.

The measured transient absorption builds up significantly more slowly than the ion population is supposed to grow according to the quasistatic ADK theory. Either due to a delayed response of the electronic rearrangement in the ion, to nonadiabatic tunneling in the rapidly-varying external field, or to the combination of both effects. Whatever applies, this attosecond experiment provides the first direct insight into *sub-atomic electron tunneling* and sets a couple-of-hundred attosecond upper limit to the response time of the atomic electron cloud to the loss of an electron.

#### XVI. SUB-ATOMIC ELECTRON OSCILLATIONS IN SLOW MOTION

The tunneling electron escapes—with comparable probability—from two different energy levels of the  $4p$  sub-shell of krypton. As a consequence, the hole in the electron cloud of the krypton ion is created in a superposition state. The resultant wave packet executes periodic oscillations, just as the electron in the  $1S-2P$  superposition state of the hydrogen atom does in Fig. 2. Zhi-Heng Loh, Eleftherios Goulielmakis, and co-workers captured these oscillations for the first time (Goulielmakis *et al.*, 2010). The attosecond XUV probe pulse can interrogate this sub-atomic motion similarly to probing its “starter gun”: tunneling ionization. By further delaying the probe with respect to the peak of the ionizing single-cycle laser pulse and recording transient absorption spectra, see Fig. 14.

The recorded spectra indeed exhibit a periodic variation with increasing delay of the XUV probe. Its 6-fs period corresponds to the 0.7-eV energy separation of the two sublevels of the  $4p$  sub-shell of krypton ions. The “film” of the evolution of the hole density distribution shown on the

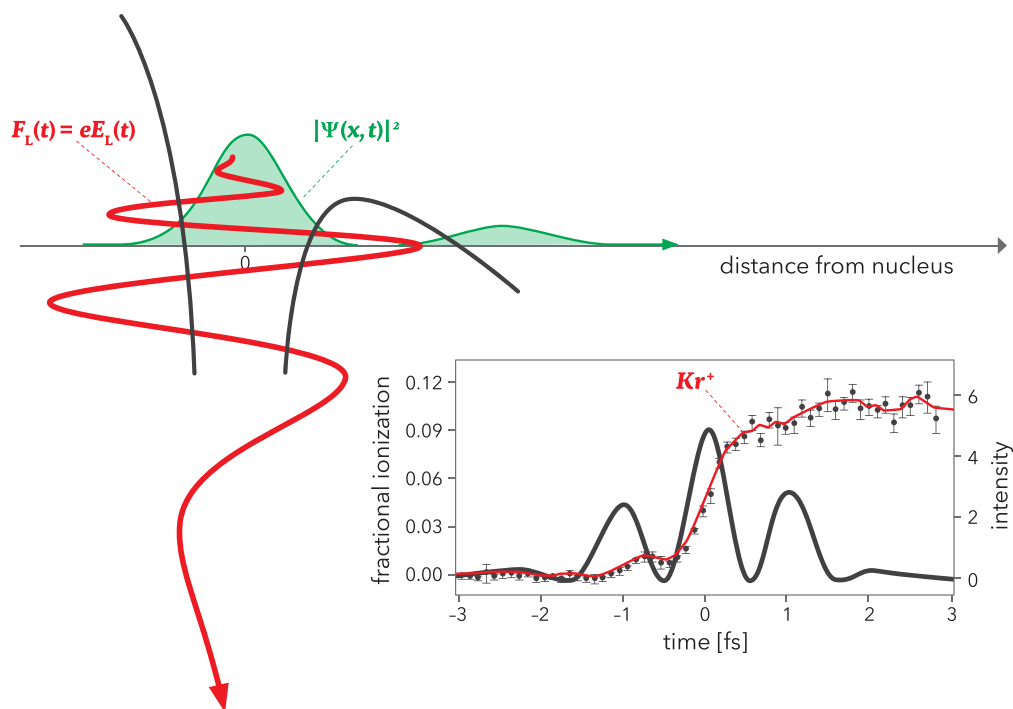


FIG. 13. Tunnel ionization of krypton atoms by a linearly polarized single-cycle near-infrared laser field probed by an attosecond XUV pulse (near 80 eV). To this end, the spectrum of the XUV pulse transmitted through the ionizing atoms in the setup of Fig. 7 was measured by a spectrometer as a function of delay between the ionizing single-cycle laser field and the attosecond XUV probe pulse. Measuring the ionization-induced change in the transmitted spectrum allowed the fraction of ions in the illuminated region to be determined at any instant during the exposure to the laser field, with a resolution of about 150 as (Wirth *et al.*, 2011).

right-hand side of Fig. 15 was “developed” from the transient absorption spectra by Nina Rohringer and Robin Santra, via modeling the interaction. The zero of time  $t_0$  has been set to coincide with the peak of the ionizing electric

field and determined by sampling the wave with the same attosecond XUV pulses via attosecond streaking; this sampling yields the instantaneous intensity evolution  $\propto E^2(t)$  shown in Fig. 14.

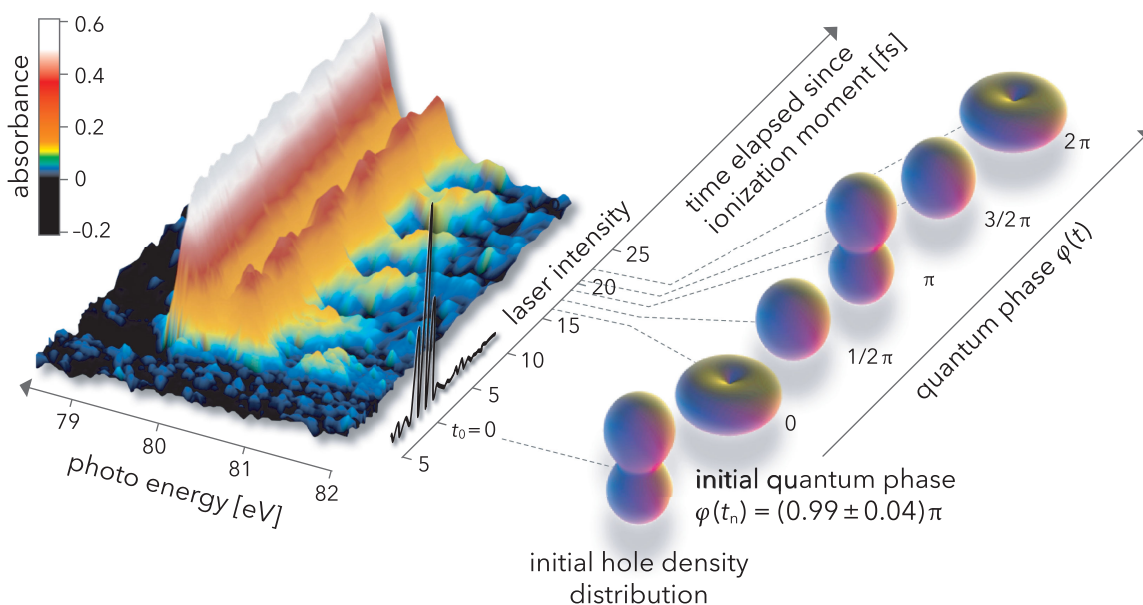


FIG. 14. Valence hole wave packet motion in krypton atoms ionized by a linearly polarized single-cycle near-infrared laser field and probed by a 150-as XUV pulse (near 80 eV). The distributions of photon energies absorbed from the attosecond XUV probe at different instants are shown in false-color representation on the left. The zero of the time axis is chosen to coincide with the peak of the cosine-shaped single-cycle laser waveform, which was simultaneously captured by attosecond streaking. Theoretical modeling of the transient absorption spectra yields the hole density distribution as a function of time as shown on the right (Wirth *et al.*, 2011).

The simultaneous use of two attosecond techniques, transient absorption spectroscopy and light-field-driven streaking, permits complete reconstruction of the sub-atomic motion following tunneling ionization. The resultant initial hole distribution at  $t_0$  is commensurate with our intuitive expectation that the hole in the electron shell is born with a shape elongated along the direction of the linearly polarized ionizing field.

Nearly a century after Schrödinger's wave equation, attosecond physics provides insight into the most intimate details of quantum mechanical motion at the sub-atomic scale.

## VII. FROM ISOLATED ATOMS TO CONDENSED MATTER

The first decade of attosecond science was marked by studies on isolated particles, mostly atoms, in the gas phase. Fundamental quantum phenomena became now accessible to human observation as they evolve in time. On an attosecond-femtosecond scale.

Modern technologies: electronics, photonics, medical diagnostics, rely, however, largely on *electronic phenomena in condensed matter*. Electronic signal processing, optical telecommunication, x-ray imaging all depend on the response of electrons to electric fields oscillating from gigahertz ( $10^9 \text{ s}^{-1}$ ) to exahertz ( $10^{18} \text{ s}^{-1}$ ) frequencies. Insight into this response may be instrumental in advancing key technologies of the 21st century.

I present two examples of how attosecond probing of the electronic response of condensed matter may foster the development of new technologies. For signal processing at optical rates and for probing human health by extracting information from vibrating molecules.

## VIII. SUB-ATOMIC MOTIONS IN CONDENSED MATTER: ELECTRIC POLARIZATION

The most fundamental consequence of any interaction between light and matter is the displacement of electronic charge density, referred to as electric polarization (briefly: polarization),

$$P(t) = en\Delta x, \quad (8)$$

where  $n$  is the electron density and  $\Delta x$  is its mean displacement induced by a linearly polarized electric field along its direction.<sup>2</sup>

In transparent materials and at moderate field strength, electrons respond almost instantaneously to the oscillations of the electric field up to frequencies of visible light. The resultant—purely electronic—motion implies an instantaneous polarization response (Fig. 15). In the infrared, energy may also be coupled to the nuclei, giving rise to their vibrations. They may well survive the excitation, leading to a retarded response.

The attosecond temporal evolution of the induced polarization  $P(t)$  along with its attosecond timing with respect to the

<sup>2</sup>For simplicity, we assumed that all electrons respond in the same way to an external field, which is generally not true. However, Eq. (8) is readily generalizable for different classes of electrons with differing polarizabilities.

driving electric field (insets in Fig. 15) determines the rate of energy exchange between light and matter (per unit volume):

$$\frac{dW}{dt} = E(t) \frac{dP}{dt} \approx E(t) \frac{dP_{\text{el}}}{dt}. \quad (9)$$

For single-cycle light fields, the polarization response *during* the laser pulse is dominated by the electronic response  $P(t) \approx P_{\text{el}}(t)$ . At vibrational resonances, the retarded response is dominated by the nuclear motion,  $P(t) \approx P_{\text{nucl}}(t)$ . This polarization radiates a coherent electromagnetic wave that temporally separates from a sudden excitation, with an electric field

$$E(t) \propto \frac{d^2 P}{dt^2} \approx \frac{d^2 P_{\text{nucl}}}{dt^2}. \quad (10)$$

Both responses occur on a sub-atomic scale, with miniscule electron displacements

$$\Delta x \ll 10^{-12} \text{ m}$$

having far-reaching implications; the energy exchange (9) related to the instantaneous electronic response is highly relevant for future optoelectronics and the radiation originating from the retarded nuclear response (10) probes the chemical environment, similarly to nuclear magnetic resonance (NMR) (Purcell, 1952).

## XIX. LIGHT-MATTER ENERGY TRANSFER IN REAL TIME

It follows from Eq. (9) that insight into light-matter energy exchange at its genuine timescale requires knowledge of  $E(t)$  and  $P(t)$ .  $E(t)$  can be acquired by attosecond streaking.  $P(t)$  is imprinted in the electric field transmitted through the sample under scrutiny. For a thin medium, referencing the transmitted to the input field allows retrieval of  $P(t)$ , which yields the polarization trace shown in Fig. 15.

The dashed line in Fig. 15 shows a near-infrared laser pulse that was passed through a thin silica sample at low and high intensities. The transmitted waveforms were measured by attosecond streaking. The difference between the normalized waveforms yields the nonlinear polarization induced by the strong field and is shown by the solid line (Sommer *et al.*, 2016).

The effective electron displacement associated with  $P_{\text{NL}}(t)$  at  $E_{\text{peak}} = 2.6 \text{ V/\AA}$  is estimated on the order of (Yakovlev, 2024)

$$\Delta x_{\text{NL}} \sim 10^{-13} \text{ m}.$$

Remarkably, even this miniscule motion leads to a substantial energy transfer.

The initial positive delay of  $P_{\text{NL}}(t)$  (left inset in Fig. 15) implies energy transfer from the field to the electrons, needed to remove them ever farther away from their field-free location. Upon returning to their equilibrium position, they radiate part of the absorbed energy back into the driving field via a negative delay of  $P_{\text{NL}}(t)$  (right inset in Fig. 15).

Figure 16 shows how this energy transfer occurs in an insulator and a semiconductor. For strong fields (near breakdown), multiphoton transitions cause a universal response that is nonreversible by the external field. For reduced field

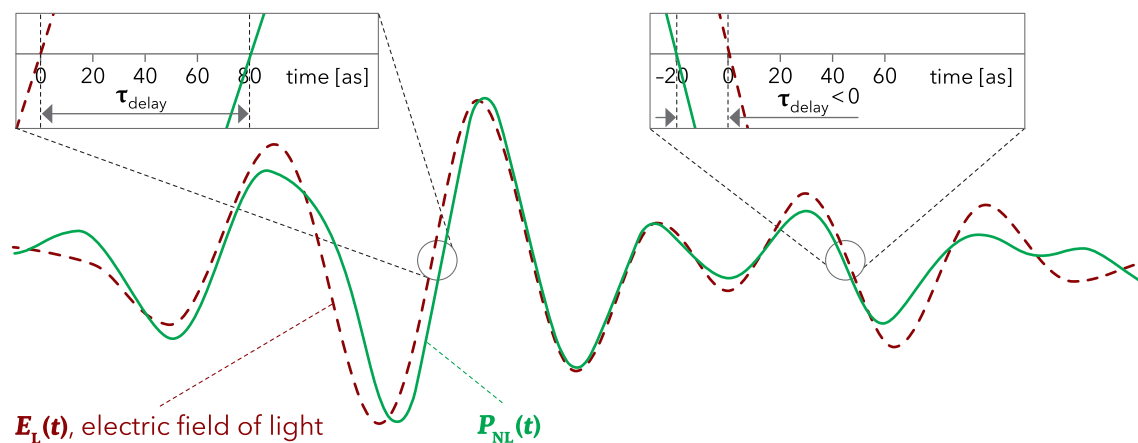


FIG. 15. Ultrashort laser field (dashed line) and the nonlinear polarization response (solid line) of a thin quartz plate for a peak electric-field strength of  $2.6 \text{ V/\AA}$  (Sommer *et al.*, 2016). The nonlinear polarization response has been evaluated from attosecond streaking of the incident and transmitted laser field. Delayed response on the leading edge of the pulse implies net energy flow from the laser field to the electronic system of the solid. The direction of energy transfer is reversed at the trailing edge, indicating that energy exchange due to the nonlinear electron-light interaction is (at least partially) reversible.

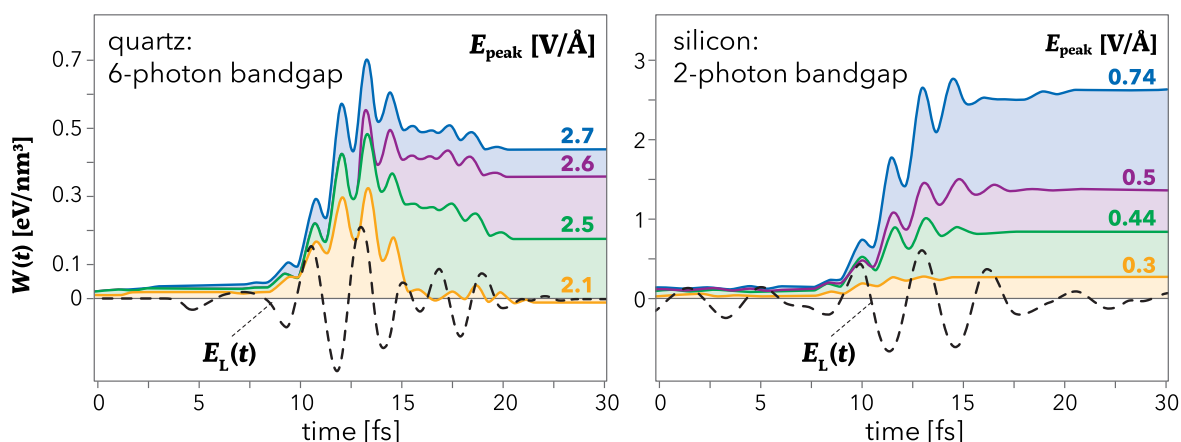


FIG. 16. Light-matter energy transfer in real time from a single-cycle laser field (dashed line) to an insulator (quartz) and a semiconductor (silicon), for different peak electric-field strengths of the incident pulse (Sommer *et al.*, 2016; Gessner, 2021).

strengths, the nonreversible part of the energy transfer related to six-photon absorption gradually disappears. The nondissipative optical Kerr effect is left behind at  $E_{\text{peak}} = 2.1 \text{ V/\AA}$ . By contrast, in a two-photon band gap (see the right panel in Fig. 16) such a regime is of field-reversible nonlinear energy transfer is completely missing (Gessner, 2021).

These studies showcase how real-time access to the energy flow between light and matter will be instrumental in exploring the optimum interaction regimes for dissipation-free high-speed signal processing in the future. However, insight into subcycle light-matter energy transfer has already borne first fruit in the presence.

## XX. PETAHERTZ REAL-TIME OSCILLOSCOPE

Real-time oscilloscopes are able to capture individual electric waveforms in the microwave regime. With bandwidth approaching 100 GHz and at a price level of a Ferrari, they define the frontiers of electronic signal metrology. Figure 17 uncovers a route to speeding up these “Ferraris of modern electronics” by more than a factor of 10 000.

Zooming into the energy-transfer evolution in quartz for the highest electric-field strength, near  $3 \text{ V/\AA}$ , within a single half of the field cycle—reveals its substantial completion during less than 0.5 fs. That is, charge carriers are injected into the conduction band within less than 0.5 fs in a single half cycle. With a properly tailored, cosine-shaped, single-cycle waveform, this charge carrier injection can be substantially confined to the central half cycle, as depicted on the right-hand side of Fig. 17. This extreme temporal confinement comes about via tunneling obeying Eq. (7) for  $E_{\text{peak}} > E_{\text{crit}}$ , see left panel of Fig. 17.

Optical-field-induced electron tunneling in a solid critically relies on—and *can only be realized with*—(near-)single-cycle light. This is because  $E_{\text{peak}} > E_{\text{crit}}$  would cause irreversible breakdown for multicycle pulses (Lenzner *et al.*, 1998).

The sub-cycle carrier injection turns an insulator into a conductor within less than 500 as. This opens the route to a simple solid-state field sampler of unprecedented—petahertz—bandwidth. By focusing the single-cycle “probe” light field along with the “test” field into a small volume between two electrodes, where the test field separates the injected electrons and holes, and drives a current through an

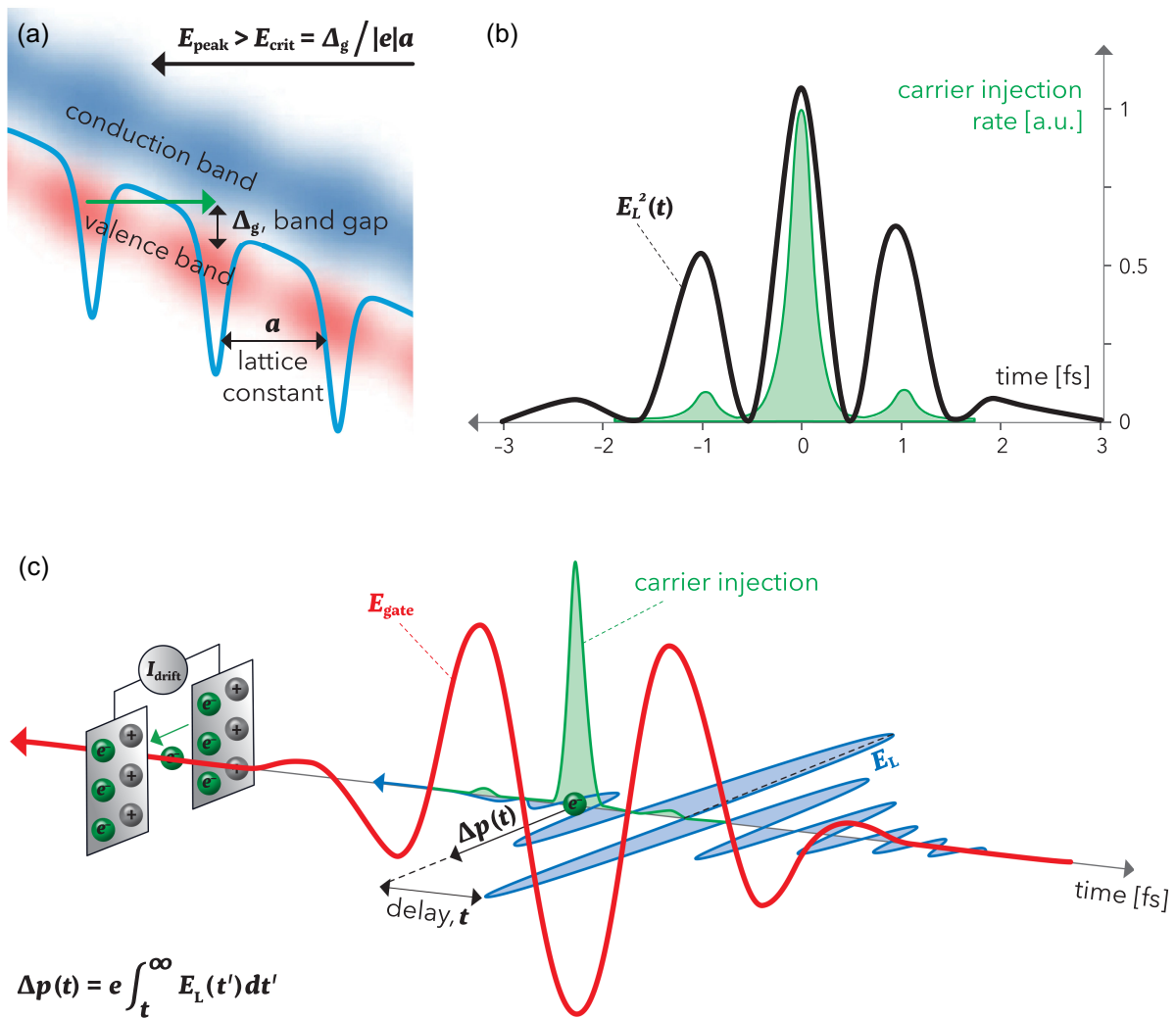


FIG. 17. (a) Optical-field-induced electron tunneling from the valence to the conduction band of a wide-gap solid is temporally confined to (b) the central half cycle of a cosine-shaped single-cycle laser field and, hence, (c) can be used for sampling the electric field of light (blue line in the horizontal plane) up to petahertz frequencies in a solid-state circuit.

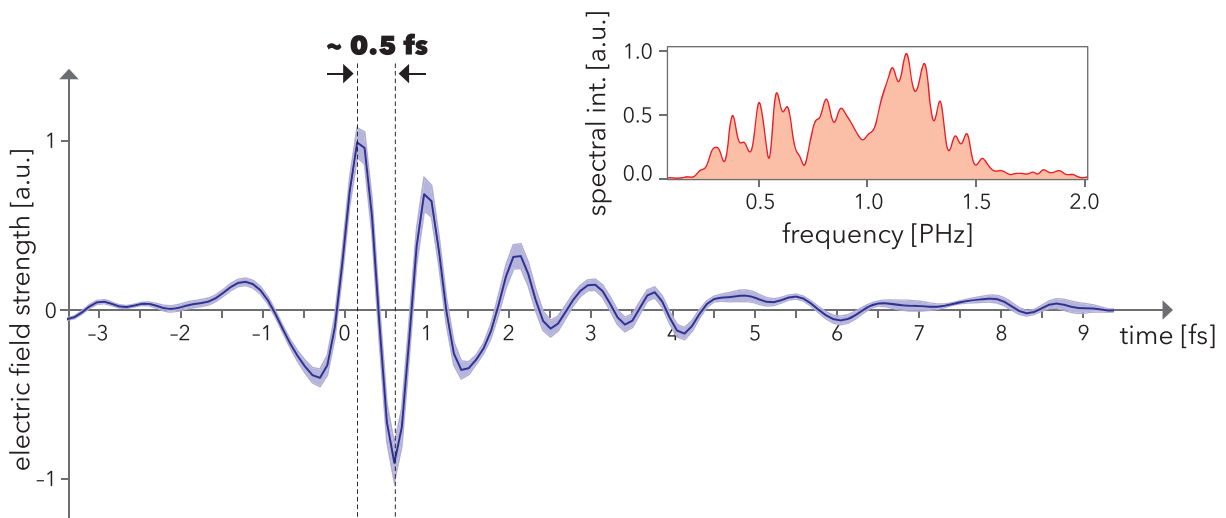


FIG. 18. Electric-field evolution of a sub-femtosecond single-cycle ultraviolet laser pulse sampled by a petahertz real-time oscilloscope (Heinzerling *et al.*, 2024).

external circuit, which is proportional to the vector potential of the test field at the moment of photoinjection (Fig. 17, lower panel). The result is a petahertz real-time oscilloscope (Sederberg *et al.*, 2020). With a noble gas between the electrodes, Amelie Heinzerling and Nick Karpowicz have recently proven its capacity to sample fields beyond 1.5 PHz (Fig. 18) (Heinzerling *et al.*, 2024). A 10 000-fold increase in bandwidth as compared to a state-of-the-art real-time oscilloscope in modern electronics.

## XXI. ATTOSECOND CONDENSED-MATTER SCIENCE

Single-cycle light from the infrared to the deep ultraviolet, along with the capability of sampling their oscillating fields (Sederberg *et al.*, 2020; Heinzerling *et al.*, 2024), provides entirely new tools for controlling and probing electron phenomena in condensed-matter with attosecond resolution. These precisely controlled fields can launch sub-femtosecond electron/hole wave packets in the conduction/valence band of band-gap materials or on molecular orbitals. The force these fields exert on electrons can be used to steer the motion of these wave packets with sub-femtosecond precision.

The unfolding electronic dynamics can be probed by the polarization they induce, which can be read out by the fields emanating from the interaction. This access is provided by solid-state instrumentation, obviating the need for complex vacuum systems.

The emerging new discipline, attosecond condensed-matter science, will foster advancing electronics to its ultimate speed limits and mediating deep dives into the composition of molecular systems.

## XXII. PROBING MOLECULES VIA SUB-ATOMIC ELECTRONIC MOTIONS

Electrons respond within tens of attoseconds to sudden external influences. This universal timescale (Breibach and Cederbaum, 2005) is reversible: with the influence being reversed (undone), the change in the electrons' quantum state disappear on the same universal attosecond timescale. This applies far from electronic resonances, for moderate field strengths and frequencies below ionization threshold. And in the absence of any motion of the nuclear backbone of molecules or solids, which we tacitly assumed in our discussions so far.

The characteristic timescale of vibrations of the nuclear backbone of biological molecules is vastly stretched, from about 100 THz down to below 1 THz. The frequencies of those vibrations are specific to the molecule in question and access to these frequencies in a molecular sample offers information about its composition. They lend themselves for molecular analytics<sup>3</sup> via inelastic scattering of visible light, the Raman effect (Raman, 1930), or by resonant absorption of infrared light. Here we focus on the latter

route, implemented with a sudden, ideally single-cycle, excitation.

The sudden excitation opens a time window for background-free detection of the coherent infrared wave emanating from the vibrating molecules. Field sampling of this molecular signal, dubbed *infrared electric-field molecular fingerprinting* (EMF), provides access to miniscule changes of the molecular composition of biological samples allows with unprecedented signal-to-noise ratio (Pupeza *et al.*, 2020).

## XXIII. EMF VERSUS NMR

There is a close analogy—both conceptually and methodologically—between nuclear magnetic resonance, NMR, and EMF. In NMR spectroscopy, a radio-frequency (RF) pulse triggers the precession of magnetic nuclei in a strong static magnetic field. Their precession induces an alternating current in a coil, which creates an RF voltage at its output ports. This NMR signal decays exponentially (free induction decay) due to loss of coherence among the precessing nuclei in the sample. The NMR signal spectrum contains the precession frequencies of the NMR-active nuclei, which depend on the local chemical environment. The microsecond-duration RF pulse induces ms-to-second-duration NMR signals.

In EMF, nuclear vibrations rather than nuclear precessions are excited. At 10 000–100 000 times higher frequencies. The EMF signal decays more than a billion times faster than the NMR signal. Consequently, the NMR signal contains  $10^4$ – $10^6$  times more field oscillation cycles than the EMF signal and—in the frequency domain—a correspondingly larger number of independent spectral channels. However, only a tiny fraction of these channels carries useful signal with chemical information. By contrast, the multi-THz bandwidth of the EMF signal is largely filled with vibrational frequencies, albeit many of them may be correlated with each other. EMF is vastly superior to NMR in terms of sensitivity. Future research will reveal whether EMF can outperform NMR in terms of the amount of molecular information about the type and quantity of functional groups present in complex biological samples.

## XXIV. SUB-ATOMIC MOTIONS PROBE HUMAN HEALTH

The electric-field molecular fingerprint responds to changes in the molecular composition of biological samples. Such alterations in human blood serum or plasma are connected to changes in the physiological state of human organism. This connection serves as a basis for the ability of specific molecular markers (biomarkers) to signal a transition from health to disease. The efficacy of detecting such a transition tends to increase with the use of multiple markers. May the infrared molecular fingerprint—as a multiparametric biomarker—be sensitive to a variety of chronic conditions? This has been the question that we started to seek the answer to in 2016 together with Mihaela Žigman, who took the lead in building a team and collaborations with several clinics of the LMU.

Among others with Jürgen Behr, Head of the Clinic of Pulmonology of the LMU, with whom Mihaela, along with Marinus Huber, Wolfgang Schweinberger, Michael Trubetskov, Kosmas Kepesidis, and others, set out to test

<sup>3</sup>Analysis of molecular content of biological samples for applications including but not limited to the protection of human health.

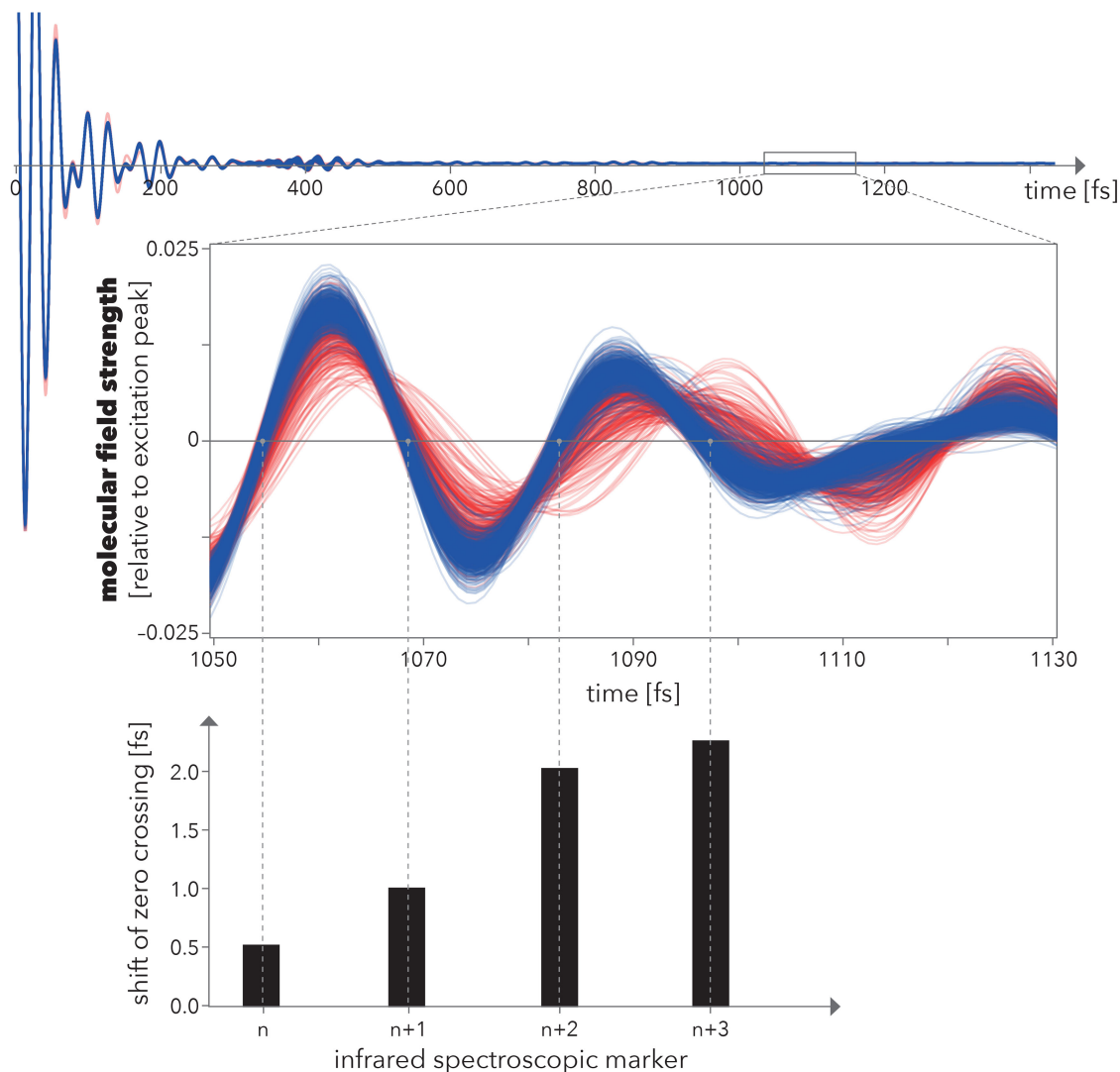


FIG. 19. Infrared electric-field molecular fingerprints of blood plasma samples of 470 patients diagnosed with non-small-cell lung cancer (cases) and 470 nonsymptomatic reference individuals (controls). The case and control groups of individuals have been matched to each other in terms of their age distribution and some other parameters. The central wavelength of the octave-spanning spectrum of the excitation pulse is  $8\ \mu\text{m}$  and its peak electric field is  $0.0008\ \text{V}/\text{\AA}$ . Inset: fingerprint signals in the temporal interval 1050–1130 fs after the excitation peak. Lower panel: mean temporal shifts of the field zero crossings of the case and controls signals infrared spectroscopic markers extracted from the time interval 1050–1130 fs after excitation.

the sensitivity of EMF to one of the chronic conditions with high mortality, lung cancer. Figure 19 shows the infrared electric-field molecular fingerprint of 470 samples of patients diagnosed with stage I–stage IV non-small-cell lung cancer and 470 well-matched cancer-free control individuals.

Quantitative differences between the two sets of traces can be analyzed in terms of two discrete samples per oscillation period, e.g., the zero crossings of the traces. Their mean differences between the case and control traces and their standard deviations are shown for a few field zero crossings in the lower panel of Fig. 19. They stand for another half thousand zero-crossing spectroscopic markers that can currently be evaluated with a satisfactory signal-to-noise ratio from EMF traces of human blood plasma. The differences in the zero-crossing markers range from tens of attoseconds to a few femtoseconds. These differences show clear monotonic

correlation with progression of the disease (from stage I to stage IV), strongly suggesting that the differences are caused by lung cancer and its concomitants rather than some other, independent health aberrations. Hence, they can be used for training an algorithm for detecting non-small-cell lung cancer; stage-by-stage classification indicates promising efficacy even for early (nonmetastatic) stages of the disease (Kepesidis *et al.*, 2024).

The peak electric field of the few-cycle midinfrared laser pulse used for the excitation of the blood plasma samples is  $E_{\text{peak}} \approx 7 \times 10^6\ \text{V}/\text{m}$ . The field strengths of the molecular signal shown in Fig. 20 are consistent with vibrationally induced effective electronic displacements of the order of

$$\Delta x_{\text{vibr}} \sim 10^{-14}\ \text{m}.$$

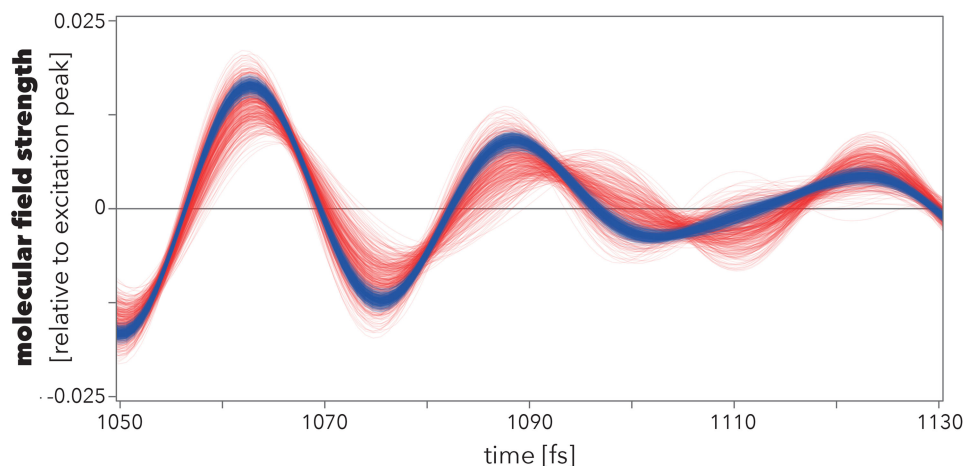


FIG. 20. Red lines: measured infrared electric-field fingerprint signals of lung cancer reproduced from the upper inset of Fig. 19. Blue lines: the same number of simulated reference signals representative for the variation within individuals over time. Referencing cancer fingerprints to controls obtained from the same individual before contracting the disease will allow more reliable early detection of health-disease transitions.

Remarkably, these *sub-picometer-scale electronic motions*, with a magnitude less than a thousandth of the size of an atom, are able to generate electric fields (Fig. 20) measurable within seconds with a signal-to-noise ratio of several hundred (Schweinberger, 2024).

## XXV. TOWARD CARING FOR HEALTH—BY MONITORING IT

The extent to which the disease-induced differences between case and control traces enable detection of the disease critically depends on their magnitude relative to the variability of control, reference individuals. This biological signal-to-noise ratio, called the *effect size*, is a quantity of critical importance in any health dataset to be used for monitoring human health, with the aim to observe health aberrations at a stage of their development when treatment can be efficient.

The effect size can be increased by improving the sensitivity of the process capturing the disease-induced signal. But it can also be increased by reducing the spread of controls. The infrared fingerprint of blood plasma has been found to be extremely stable over time in healthy individuals, with a variation that is typically by 2.5 smaller for any person than its spread between different healthy individuals (Huber *et al.*, 2021). If each individual cancer fingerprint could be referenced to a set of control fingerprints collected from the same person before contracting the disease, the spread of references would shrink, as illustrated in Fig. 20. Simulations indeed indicate that the greatly reduced spread of controls improves the efficacy of spotting early-stage lung cancer (Eissa, Huber, and Kepesidis, 2024). This suggests that following up individuals with a regular blood test may contribute to protecting their health and provided an incentive for rolling out a longitudinal study with 15 000 volunteers in Hungary<sup>4</sup> at the Center for Molecular Fingerprinting.<sup>5</sup>

<sup>4</sup>See <http://www.h4h.hu>.

<sup>5</sup>See <http://www.cmf.hu>.

Our efforts are driven by a vision:

*Imagine a tool that could catch issues before they become significant problems. Early disease diagnostics are a bit like a sensitive radar, but one that is affordable to everyone and is fast and easy to use. The goal is to detect irregularities well before individuals get symptoms or would even think about seeing a doctor for clarification, at which point it might be too late to intervene, as is the case for many cancers. This is a strategy to nip potential health hiccups in the bud, promising help to keep us on the road to well-being. But only if there is a medical treatment strategy available to deal with that very hiccup (Žigman, 2024).*

Successful pursuit of this vision will also stimulate developing new treatment strategies benefiting from early detection.

## XXVI. OUR PATH

Is it worthwhile to capture electronic motion? A nontrivial question, if requiring decades of effort to be realized.

My answer was a determined “yes,” which, in turn, gave rise to a genesis of specific questions: **Q1**, and then **Q2**, and then **Q3**.

They provided guidance and assistance in making decisions. And created an inexhaustible source of motivation over the years.

Where are we now? In the process of seeking answer to **Q3**: which application appears to be most rewarding?

Given that every year, 17 million people under the age of 70 die of noncommunicable diseases, most of which are preventable,<sup>6</sup> we—at attoworld<sup>7</sup>—feel inspired and motivated to

<sup>6</sup>See <http://www.who.int/publications/i/item/9789240057661>.

<sup>7</sup>See <http://www.attoworld.de> and <http://www.cmf.hu>.

seek answers to the questions (without knowing whether the quest for answers will be rewarding):

What is the most economically viable set of health data that enables comprehensive and dependable monitoring of human health ..... and to what extent can controlled light contribute to their acquisition?

It is telling how scientific research triggered by curiosity about electronic motions has led to this question.

## XXVII. OTHER PATHS

Attosecond science emerged from decades of advancements in laser technology and fundamental physics concepts. From the initial observation of the electron's wave nature to the development of tools to control electron motions, this field has revolutionized our understanding of the ultrafast world. With continued innovation, attosecond science promises to unlock new frontiers in electronics, materials science, medicine, and beyond. Opening many more paths to be pursued.



Courtesy of M. Zigman and D. Luck.

## ACKNOWLEDGMENTS

I thank Vlad Yakovlev for his help in the final shaping of the manuscript and Nick Karpowicz and Nicole Buchwiser for carefully reading it.

## REFERENCES

- Ammosov, M. V., N. B. Delone, and V. P. Krainov, 1986, “Tunnel ionization of complex atoms and of atomic ions in an alternating electromagnetic field,” *Zh. Eksp. Teor. Fiz.* **91**, 2008–2013 [*Sov. Phys. JETP* **64**, 1191 (1986)], <http://jetp.ras.ru/cgi-bin/e/index/e/64/6/p1191?a=list>.
- Baltuska, A., *et al.*, 2003, “Attosecond control of electronic processes by intense light fields,” *Nature (London)* **421**, 611.
- Bardeen, J., 1956, “Semiconductor research leading to the point contact transistor,” <https://www.nobelprize.org/uploads/2018/06/bardeen-lecture.pdf>.
- Bloembergen, N., 1981, “Nonlinear optics and spectroscopy,” <https://www.nobelprize.org/uploads/2018/06/bloembergen-lecture.pdf>.
- Born, M., 1954, “The statistical interpretation of quantum mechanics,” <https://www.nobelprize.org/uploads/2018/06/born-lecture.pdf>.
- Breidbach, J., and L. S. Cederbaum, 2005, “Universal Attosecond Response to the Removal of an Electron,” *Phys. Rev. Lett.* **94**, 033901.
- Cavaliere, A., *et al.*, 2007, “Attosecond spectroscopy in condensed matter,” *Nature (London)* **449**, 1029.
- Christov, I. P., M. M. Murnane, and H. C. Kapteyn, 1997, “High-Harmonic Generation of Attosecond Pulses in the ‘Single-Cycle’ Regime,” *Phys. Rev. Lett.* **78**, 1251.
- Compton, A. H., 1923, “A quantum theory of the scattering of x-rays by light elements,” *Phys. Rev.* **21**, 483.
- Corkum, P. B., 1993, “Plasma Perspective on Strong Field Multiphoton Ionization,” *Phys. Rev. Lett.* **71**, 1994–97.
- Davisson, C., and L. H. Germer, 1927, “The scattering of electrons by a single crystal of nickel,” *Nature (London)* **119**, 558.
- de Broglie, L., 1929, “The wave nature of the electron,” <https://www.nobelprize.org/uploads/2016/04/broglie-lecture.pdf>.
- Drescher, M., M. Hentschel, R. Kienberger, M. Uiberacker, V. Yakovlev, A. Scrinzi, Th. Westerwalbesloh, U. Kleineberg, U. Heinzmann, and F. Krausz, 2002, “Time-resolved atomic inner-shell spectroscopy,” *Nature (London)* **419**, 803.
- Eissa, T., M. Huber, and K. Kepsidis, 2024 (private communication).
- Faraday, M., 1834, “On electrical decomposition,” *Phil. Trans. R. Soc. London* **124**, 77–122.
- Fowler, R. H., and L. Nordheim, 1928, “Electron emission in intense electric fields,” *Proc. R. Soc. A* **119**, 173.
- Gessner, J., 2021, “Strong-field driven charge and spin dynamics in solids,” Ph.D. thesis (Ludwig-Maximilian-Universität München).
- Goulielmakis, E., *et al.*, 2004, “Direct measurement of light waves,” *Science* **305**, 1267–1269.
- Goulielmakis, E., *et al.*, 2008, “Single-cycle nonlinear optics,” *Science* **320**, 1614–1617.
- Goulielmakis, E., *et al.*, 2010, “Real-time observation of valence electron motion,” *Nature (London)* **466**, 739.
- Hänsch, T. W., 2005, “Passion for precision,” <https://www.nobelprize.org/uploads/2018/06/hansch-lecture.pdf>.
- Heinzerling, A., F. Tani, M. Agarwal, V. S. Yakovlev, F. Krausz, and N. Karpowicz, 2024, “Field-resolved attosecond solitons,” (to be published).
- Huber, M., K. V. Kepsidis, L. Voronina, M. Božić, M. Trubetskov, N. Harbeck, F. Krausz, and M. Žigman, 2021, “Stability of person-specific blood-based infrared molecular fingerprints opens up prospects for health monitoring,” *Nat. Commun.* **12**, 1511.
- Itatani, J., F. Quéré, G. L. Yudin, M. Yu. Ivanov, F. Krausz, and P. B. Corkum, 2002, “Attosecond Streak Camera,” *Phys. Rev. Lett.* **88**, 173903.
- Keldysh, L. V., 1964, “Ionization in the field of a strong electromagnetic wave,” *Zh. Eksp. Teor. Fiz.* **47**, 1945 [*Sov. Phys. JETP* **20**, 1307 (1965)], <http://jetp.ras.ru/cgi-bin/e/index/e/20/5/p1307?a=list>.
- Kepsidis, K., *et al.*, 2024 (in preparation).
- Kienberger, R., *et al.*, 2004, “Atomic transient recorder,” *Nature (London)* **427**, 817–821.
- Kitzler, M., N. Milosevic, A. Scrinzi, F. Krausz, and T. Brabec, 2002, “Quantum Theory of Attosecond XUV Pulse Measurement by Laser Dressed Photoionization,” *Phys. Rev. Lett.* **88**, 173904.
- Krause, M. O., and J. H. Oliver, 1979, Natural widths of atomic  $K$ , and  $L$  levels,  $K\alpha$  x-ray lines and several  $KLL$  Auger lines,” *J. Phys. Chem. Ref. Data* **8**, 329.
- Krausz, F., and M. Ivanov, 2009, “Attosecond physics,” *Rev. Mod. Phys.* **81**, 163–234.
- Lenzner, M., J. Krüger, S. Sartania, Z. Cheng, Ch. Spielmann, G. Mourou, W. Kautek, and F. Krausz, 1998, “Femtosecond Optical Breakdown in Dielectrics,” *Phys. Rev. Lett.* **80**, 4076.
- Lewenstein, M., Ph. Balcou, M. Yu. Ivanov, A. L’Huillier, and P. B. Corkum, 1994, “Theory of high-harmonic generation by low-frequency laser fields,” *Phys. Rev. A* **49**, 2117–2132.
- Li, X. F., A. L’Huillier, M. Ferray, L. A. Lompré, and G. Mainfray, 1989, “Multiple-harmonic generation in rare gases at high laser intensity,” *Phys. Rev. A* **39**, 5751.
- Maiman, T. H., 1960, “Stimulated optical radiation in ruby,” *Nature (London)* **187**, 493.
- Mairesse, Y., and F. Quéré, 2005, “Frequency-resolved optical gating for complete reconstruction of attosecond bursts,” *Phys. Rev. A* **71**, 011401(R).
- Moseley, H. G. J., 1913, “The high-frequency spectra of elements,” *Philos. Mag. Ser. 6* **26**, 1024–1034.
- Moulton, P. F., 1986, “Spectroscopic and laser characteristics of  $\text{Ti:Al}_2\text{O}_3$ ,” *J. Opt. Soc. Am. B* **3**, 125.
- Neppel, S., *et al.*, 2015, “Direct observation of electron propagation and dielectric screening on the atomic length scale,” *Nature (London)* **517**, 342.
- Nisoli, M., S. De Silvestri, O. Svelto, R. Szipöcs, K. Ferencz, Ch. Spielmann, S. Sartania, and F. Krausz, 1997, “Compression of high-energy pulses below 5 fs,” *Opt. Lett.* **22**, 522.
- Pupeza, I., *et al.*, 2020, “Field-resolved infrared spectroscopy of biological systems,” *Nature (London)* **577**, 52.
- Purcell, E. M., 1952, “Research in nuclear magnetism,” <https://www.nobelprize.org/uploads/2018/06/purcell-lecture.pdf>.
- Raman, C. V., 1930, “The molecular scattering of light,” <https://www.nobelprize.org/uploads/2018/06/raman-lecture.pdf>.
- Russell, P., 2003, “Photonic crystal fibers,” *Science* **299**, 358.
- Schrödinger, E., 1926, “An undulatory theory of the mechanics of atoms and molecules,” *Phys. Rev.* **28**, 1049.
- Schrödinger, E., 1933, “The fundamental idea of wave mechanics,” <https://www.nobelprize.org/uploads/2017/07/schrodinger-lecture.pdf>.
- Schultze, M., *et al.*, 2010, “Delay in photoemission,” *Science* **328**, 1658–1662.
- Schweinberger, W., 2024 (private communication).
- Sederberg, S., *et al.*, 2020, “Attosecond optoelectronic field measurement in solids,” *Nat. Commun.* **11**, 430.
- Siegbahn, M., 1925, “The x-ray spectra and the structure of the atoms,” <https://www.nobelprize.org/uploads/2018/06/siegbahn-lecture.pdf>.

- Sommer, A., *et al.*, 2016, “Attosecond nonlinear polarization and light-matter energy transfer in solids,” *Nature (London)* **534**, 86.
- Spence, D. E., P. N. Kean, and W. Sibbett, 1991, “60-fs pulse generation from a self-mode-locked Ti:sapphire laser,” *Opt. Lett.* **16**, 42–44.
- Spielmann, Ch., N. H. Burnett, S. Sartania, R. Koppitsch, M. Schnürer, C. Kan, M. Lenzner, P. Wobrauschek, and F. Krausz, 1997, “Generation of coherent x-rays in the water window using 5-femtosecond laser pulses,” *Science* **278**, 661–664.
- Stingl, A., C. Spielmann, F. Krausz, and R. Szipőcs, 1994, “Generation of 11-fs pulses from a Ti:sapphire laser without the use of prisms,” *Opt. Lett.* **19**, 204.
- Strickland, D., and G. Mourou, 1985, “Compression of amplified chirped optical pulses,” *Opt. Commun.* **56**, 219.
- Szipőcs, R., K. Ferencz, Ch. Spielmann, and F. Krausz, 1994, “Chirped multilayer coatings for broadband dispersion control in femtosecond lasers,” *Opt. Lett.* **19**, 201.
- Thomson, G. P., and A. Reid, 1927, “Diffraction of cathode rays by a thin film,” *Nature (London)* **119**, 890.
- Townes, C. H., 1964, “Production of coherent radiation by atoms and molecules,” <https://www.nobelprize.org/uploads/2018/06/townes-lecture.pdf>.
- Uiberacker, M., *et al.*, 2007, “Attosecond real-time observation of electron tunnelling in atoms,” *Nature (London)* **446**, 627–632.
- van der Waals, J. D., 1910, “The equation of state for gases and liquids,” <https://www.nobelprize.org/uploads/2018/06/waals-lecture.pdf>.
- Wirth, A., *et al.*, 2011, “Synthesized light transients,” *Science* **334**, 195.
- Xu, L., T. W. Hänsch, Ch. Spielmann, A. Poppe, T. Brabec, and F. Krausz, 1996, “Route to phase control of ultrashort light pulses,” *Opt. Lett.* **21**, 2008–2010.
- Yakovlev, V. S., J. Gagnon, N. Karpowicz, and F. Krausz, 2010, “Attosecond Streaking Enables the Measurement of Quantum Phase,” *Phys. Rev. Lett.* **105**, 073001.
- Yakovlev, Vladislav, 2024 (private communication).
- Žigman, M., 2024, “From ancient wisdom to modern technologies,” *Pulse* **4**, 6–9, [https://www.attoworld.de/fileadmin/user\\_upload/tx\\_attoworld/News/NewsLetter/Content/2023\\_24\\_V04\\_Newsletter.pdf](https://www.attoworld.de/fileadmin/user_upload/tx_attoworld/News/NewsLetter/Content/2023_24_V04_Newsletter.pdf).